This is a non-peer-reviewed preprint submitted to EarthArXiv. This work has been submitted to Chemical Geology.

Title: A First Principles Critique of the Back Calculation Method: Understanding and Assessing the Alteration of Atmospheric Gases Trapped in Ancient Fluid Inclusions

Authors: Justin G. Park^{1,2*}, Morgan F. Schaller^{1,2}

Affiliations:

- 1. Department of Earth and Environmental Sciences, Rensselaer Polytechnic Institute, Troy, New York. 12180
- 2. Center for Environmental and Stable Isotope Analysis, Rensselaer Polytechnic Institute, Troy, New York. 12180

Contact: Parkj17@rpi.edu, Schall@rpi.edu

Address: Science Center 110 8th St. Troy, NY. 12180

Abstract:

The extraction of atmospheric gases from fluid inclusions has emerged as an extremely promising approach for directly constraining the composition of Earth's ancient atmospheres. However, the veracity of data obtained from these inclusions critically depends on how well one can account for the effects of physical chemistry and post-depositional alteration. The Back Calculation Method (BCM) attempts to discern unaltered atmospheric compositions from variably modified inclusion gases, primarily O₂ and CO₂, but fails to account for the effects of gas solubility. Moreover, the method lacks an explicit mathematical formulation, and limited articulation of its implicit assumptions and limitations has introduced ambiguity in the interpretation of reconstructed atmospheric compositions. From first principles, we derive the formulation underlying the BCM and use it to formally evaluate the limitations of the method. We expand this framework to include the variable effects of gas solubility and incorporate recent techniques to partition inclusion volatiles trapped in the gaseous and aqueous phases. In reexamining modern inclusion gases, we find evidence of heterogeneous entrapment of gas and brine, as well as variable alteration extents and pathways. These observations violate the core assumptions of the BCM, suggesting the technique has been applied inappropriately to ancient samples and that their interpreted atmospheric compositions require thorough reevaluation. We conclude by demonstrating carbon isotope measurements of inclusion CO₂ can incorporated to assess the extent of gas alteration and provide an outline for future work intending to reconstruct atmospheric compositions from these inclusions.

1.0 Introduction

Fluid inclusions in surficial minerals have emerged as valuable archives for directly investigating the evolution of Earth's atmosphere and surface environments through time. Mineral phases that precipitate in equilibrium with the atmosphere can capture and preserve chemical signatures of the overlying atmosphere, often entrapping both air bubbles and airsaturated brines (ASB). Following careful scrutiny, samples containing primary inclusions may be selected for gas analysis (Blamey and Brand, 2019; Park and Schaller, 2025), where the trapped gases are released systematically through mechanical or thermal decrepitation, and their compositions and isotope ratios are quantified via mass spectrometry (Pettitt and Schaller, 2020). This methodology has been applied to a variety of ancient materials, including hydrothermal quartz (Avice et al., 2018; Marty et al., 2013), cherts (Pettitt et al., 2020; Sano and Pillinger, 1990), various evaporites (Blamey et al., 2016; Brand et al., 2021; Freyer and Wagener, 1975; Park et al., Accepted) and even organic amber matrices (Berner and Landis, 1988; Landis and Berner, 2018). These samples provide the rare opportunity to directly measure atmospheric gases from millions, or even billions, of years ago, extending well beyond the capabilities of ice core records (Bauska, 2025; Raynaud et al., 2020). While these samples may be temporally sparse, this method provides a significant advantage over the numerous, and often conflicting, proxies that attempt to indirectly constrain atmospheric composition and evolution (The Cenozoic CO2 Proxy Integration Project (CENCO2PIP) Consortium, 2023).

While the merit of these studies is clear, direct gas analyses are not without limitations, especially in the interpretation of the bulk composition of the volatiles released during decrepitation. Bulk atmospheric compositions are typically inferred from the quantification of the major atmospheric species such as N₂, O₂, Ar, and CO₂, and occasionally minor gases including CH₄, H₂, and He. Ideally, the relative abundances of these gases will be consistent between samples of similar origin, at least within the bounds of analytical uncertainty. However, gas compositions often vary significantly beyond these limits, and post entrapment alteration is frequently levied to explain such variance. For example, studies of atmospheric gases in fossil amber have shown that O₂ reacts with the organic amber matrix, as well as the CH₄, H₂, and CO₂ rich gases exuded by the original tree (Berner and Landis, 1988; Landis and Berner, 2018), consuming O₂ and creating oxidized organic species *in situ*. Similar alteration pathways have been proposed for halite fluid inclusions, where O₂ is thought to react with Organic Matter decomposition Gases, namely CO₂ and CH₄, whimsically abbreviated as OMG (Blamey and Brand, 2019).

A common feature of these studies is the attempt to back-calculate unaltered atmospheric compositions based on observable patterns within the ratios of the gases, in particular the oxidative reactions involving the consumption of O₂ and production of CO₂. The back calculation method (BCM) attempts to determine these values by fitting linear regressions

between the relative abundances of two or more gases (e.g., O₂ versus CO₂ for fossil ambers, and O₂ versus OMG for halite inclusions) (Berner and Landis, 1988; Blamey and Brand, 2019; Landis and Berner, 2018). Regressions are interpreted to reflect either the degree of post entrapment alteration, or the mixing of two distinct endmembers in the case of the ambers. The intercept of these regressions is interpreted to be equivalent to the unaltered gas end member, which often is viewed as representative of the atmosphere (Fig. 1). In the case of halite inclusions, the BCM has become a prominent method for determining ancient atmospheric oxygen levels (Blamey and Brand, 2019; Brand et al., 2021; Davis, 2018; Shaver, 2018).

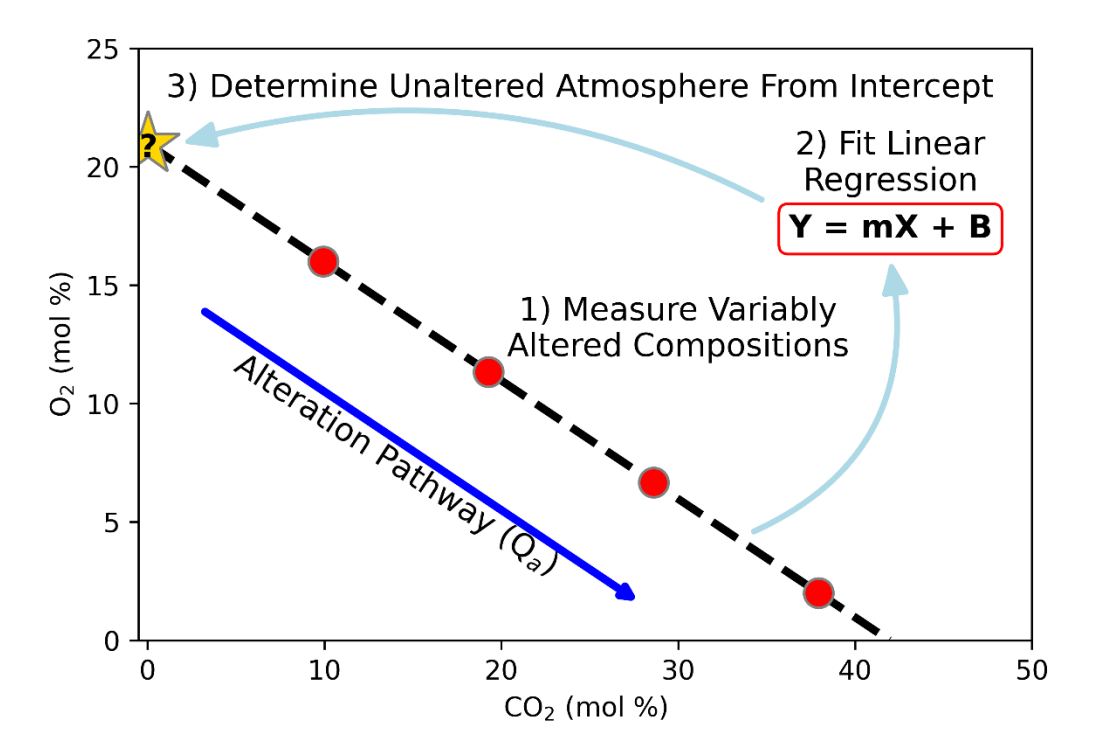


Figure. 1: A conceptual diagram outlining the application of the back calculation method as incorporated in studies of inclusion gases (e.g. see Berner and Landis, 1988; Blamey and Brand, 2019; Brand et al., 2021; Landis and Berner, 2018). The gases released from fluid inclusions are assumed to be altered to various extents from an initial atmospheric composition. A linear regression is fit between the released O_2 and CO_2 contents. The intercept of this regression is interpreted as O_2 contents of the atmosphere.

However, concerns regarding the large and often non-overlapping uncertainties between samples of the same age, as well as apparent overestimations of O₂ levels relative to proxies or the modern atmosphere, have hindered the general acceptance of results produced through this method (Mills et al., 2023). Moreover, the absence of an explicit mathematical formulation and limited articulation of the implicit assumptions behind the BCM have led to considerable ambiguity in how results are interpreted. Nor is it inherently clear what the limitations of the BCM are, and more specifically when the method *can* and *cannot* be applied. Considering these concerns, a thorough evaluation of the BCM and its theoretical basis is overdue.

Here we use first principles to derive a mathematical formulation describing the behavior of O₂ and CO₂ under the key assumptions of the BCM. This includes two major assumptions specific to the method: 1) The fluid inclusions initially captured a single, representative atmospheric composition; 2) Compositional variability reflects alteration affecting only the gases of interest. Separately, this includes a third major assumption implicit to nearly all inclusion studies: 3) the inclusions have remained closed systems since the time of entrapment (i.e. conforming to Roedder's rules (Roedder, 1984a)). By explicitly addressing these assumptions, we robustly identify limitations in the applicability of the BCM and evaluate how the method has been misapplied to real datasets. Furthermore, we advance the method by incorporating partitioning techniques that account for additional variability introduced from gas-aqueous equilibria (Park and Schaller, 2025). We conclude this study with recommendations for addressing variability introduced through phase chemistry and post-depositional alteration, and for reevaluating datasets where the BCM has been applied erroneously.

2.0 Building a Theoretical Framework for the BCM

In the following derivation, several similar terms are introduced that could lead to confusion. For clarity, we define here our nomenclature as it is applied below. We use superscript *t* to denote the value of a variable at the time of entrapment. Similarly, superscript * denotes the value of a variable after alteration has occurred, i.e., at the time of measurement.

Inclusions forming in equilibrium with the atmosphere will have gas compositions dictated by the properties of the atmosphere and the inclusion fluids. The moles of each gas trapped within the inclusion (n_i^t) is dependent on the relative volumes of atmosphere and air saturated brine. Park and Schaller (2025) model this scenario by combining the ideal gas law and Henry's law to represent the amount of a gas trapped in each phase:

$$n_i^t = P_i V \left(\frac{\varphi_g}{RT} + \left(1 - \varphi_g \right) H_S^i(T, S) \right)$$
 Eq. 1

84 For simplicity, we set:

$$Y_i\left(\varphi_g, T, S\right) = \left(\frac{\varphi_g}{RT} + \left(1 - \varphi_g\right) H_S^i(T, S)\right)$$
 Eq. 2

where P_i is the atmospheric partial pressure of the gas, V is the inclusion's volume, φ_g is the fraction of that volume occupied by an air bubble (i.e. the gas volume fraction), R is the ideal gas constant, T is the entrapment temperature, and H^i_s is the Henry's constant of the gas, which is dependent on the salinity and temperature of the fluid (Sander, 2023). Mole fractions are computed by normalizing the amount of moles of a gas to the total moles of gas trapped in the inclusion (n_{tot}^t) :

$$X_{i}^{t} = \frac{P_{i}Y_{i}\left(\varphi_{g}, T, S\right)}{\sum_{j \in J} P_{j}Y_{j}\left(\varphi_{g}, T, S\right)} = \frac{n_{i}^{t}}{n_{tot}^{t}}$$
 Eq. 3

Where *J* is the set of relevant atmospheric gases. Post entrapment alteration changes the abundance of the affected gases, which may alter their mole fractions following:

$$X_i^* = \frac{n_i^t + \Delta n_i}{n_{tot}^t + \sum_{i \in I} \Delta n_i}$$
 Eq. 4

95

For this derivation, we consider cases where only O_2 and CO_2 are altered. Similar to the respiratory quotient, the ratio of the two Δn values is described by an alteration quotient, Q_a :

$$\Delta n_{O_2} = \Delta n_{CO_2} Q_a$$
 Eq. 5

98

99 The altered mole fractions of O₂ and CO₂ are thus represented as:

$$X_{O_2}^* = \frac{n_{O_2}^t + \Delta n_{CO_2} Q_a}{n_{tot}^t + \Delta n_{CO_2} (1 + Q_a)}$$
 Eq. 6

100

101 And

$$X_{CO_2}^* = \frac{n_{CO_2}^t + \Delta n_{CO_2}}{n_{tot}^t + \Delta n_{CO_2}(1 + Q_a)}$$
 Eq. 7

102

Both equations can independently be solved for Δn_{CO_2} :

$$\Delta n_{CO_2} = \frac{X_{O_2}^* n_{tot}^t - n_{O_2}^t}{Q_a - X_{O_2}^* (1 + Q_a)}$$
 Eq. 8

104

$$\Delta n_{CO_2} = \frac{X_{CO_2}^* n_{tot}^t - n_{CO_2}^t}{1 - X_{CO_2}^* (1 + Q_a)}$$
 Eq. 9

105

106 After dividing both equations by n_{tot}^t and substituting in the appropriate forms of equation 3 we obtain the form:

$$\frac{X_{O_2}^* - X_{O_2}^t}{Q_a - X_{O_2}^* (1 + Q_a)} = \frac{X_{CO_2}^* - X_{CO_2}^t}{1 - X_{CO_2}^* (1 + Q_a)}$$
 Eq. 10

108

By solving this equation for $X_{O_2}^*$, a linear relationship between $X_{O_2}^*$ and $X_{CO_2}^*$ is found:

$$X_{O_2}^* = \frac{X_{CO_2}^* \left[X_{O_2}^t (Q_a + 1) - Q_a \right] + \left[X_{CO_2}^t Q_a - X_{O_2}^t \right]}{X_{CO_2}^t (Q_a + 1) - 1}$$
 Eq. 11

This result matches the expectations of the BCM. The slope (*m*) and intercept of this line (*b*) can be defined as:

$$m = \frac{X_{O_2}^t(Q_a+1) - Q_a}{X_{CO_2}^t(Q_a+1) - 1}$$
 Eq. 12

114 and

$$b = \frac{X_{CO_2}^t Q_a - X_{O_2}^t}{X_{CO_2}^t (Q_a + 1) - 1}$$
 Eq. 13

Both terms are dependent on the alteration quotient and the original trapped mole fractions of O_2 and CO_2 . Q_a can be isolated by dividing equation 12 by 13 and rearranging:

$$Q_a = \frac{X_{O_2}^t(m+b)}{X_{CO_2}^t m - X_{O_2}^t b + b}$$
 Eq. 14

Since the linear regression incorporates all degrees of alteration, by definition, the original trapped mole fractions must also exist on the same line, such that:

$$X_{O_2}^t = mX_{CO_2}^t + b$$
 Eq. 15

122 This allows equation 14 to be simplified to its final form:

$$Q_a = \frac{m+b}{1-b}$$
 Eq. 16

This result shows that, from a linear regression between X_{O_2} and X_{CO_2} , one can calculate an apparent value of Q_a . The estimated value provides a useful descriptor of the stoichiometric relationship between the two altered gases, which can be used to identify relevant mechanisms of alteration. Our derivation is framed specifically in terms of O_2 and CO_2 , but the mathematical structure applies equally to any two gases, or to combinations of gases, such as O_2 versus the total OMG content. However, as discussed below, the alteration quotient is more physically meaningful when applied directly to the O_2 - CO_2 system. A proper incorporation of three or more gases requires expansion of this framework and a more rigorous mathematical formulation. Such relationships are typically non-linear, as additional degrees of freedom are introduced.

3.0 Discussion

133

140

141

142

143

144

145

146

147148

149

150

151

152

153

154155

156

157

158159

160

161

162

163

164

165166

167

168

169

170

Although not previously expressed in explicit mathematical terms, the formulation presented here captures the underlying logic of the BCM as it has been applied to halite and amber inclusion gases (Blamey and Brand, 2019; Landis and Berner, 2018). By formalizing this approach, we provide a mathematical basis to assess when, and under what conditions, the BCM can be applied. In the sections below, we identify several challenges to the implicit assumptions of the BCM, which limit its broader applicability.

3.1 Mathematical Artifacts Associated with Calculating Mole Fractions

Absent of diffusive loss or addition, fluid inclusions are physically closed systems. Elemental abundances within inclusions are immutable, apart from elements gained or transformed through radioactive decay. However, inclusion gases are reactive components that are free to separate or combine with other species, such that the molecular composition changes (Pingitore and Engle, 2022). The BCM attempts to link the relative abundance of two inclusion gases through distinct alteration pathways. Yet, alteration acts on absolute quantities (moles), with only indirect influence on relative proportions (mole fractions). When expressed as mole fractions, inclusion gases are subject to the mathematical closure constraint; that is, they are bounded between 0 and 1 and always sum to unity. These constraints introduce mathematical artifacts and spurious correlations that must be carefully considered when evaluating the relationships between gases using the BCM. Principal among these concerns is a lack of independence (Aitchison, 1982): one gas cannot vary freely without affecting the others. As a result, the most abundant gases (e.g., N₂) tend to compensate the most for changes in CO₂, potentially inflating the apparent strength of their correlation. This effect is evident in nearly all modern halite samples, where R² values consistently increase as more abundant gases are compared against CO₂ (i.e., in order of increasing correlation coefficient: Ar \rightarrow O₂ \rightarrow N₂, Figs. S1-S8). Conversely, a higher R² does not necessarily imply that the variance is isolated to the two gases being compared (Chayes, 1960), despite this being a critical assumption of the BCM. The closure constraint further implies that the true center of a set of compositions is not the arithmetic mean of the components, but rather the closed geometric mean (i.e. the Aitchison center; Aitchison, 1982).

Critically, mathematical closure imparts nuance in interpreting regressions between gas mole fractions. Landis and Berner (2018) suggest the slope of an O_2 vs. CO_2 regression provides useful information to track O_2 consumption. However, this interpretation is only partially complete, as the slope is itself influenced by the closure constraint, whereas Q_a is not. The only case where the two are equal is when they are both -1, a condition that implies no net change in the total moles of gas. While negative slopes are often interpreted as evidence of a negative correlation between O_2 and CO_2 , this isn't a requirement. Q_a can be positive (i.e., both gases change in the same direction) if the intercept is greater than the absolute value of the slope (assuming the intercept falls between 0 and 1, see Equation 17). This also applies when $Q_a = 0$, a

scenario where the regression passes through 100% CO₂. When Q_a approaches zero, regressions 172 offer limited value beyond simply renormalizing the data to exclude CO₂. As CO₂ increases, the closure constraint compresses the possible values for the remaining gases, introducing heteroscedasticity into the data (i.e. unequal variance attributable to the progressive reduction of compositional space) (Chen et al., 2018). These points may also artificially flatten the slope of a regression and either increase or decrease its apparent predictive strength.

3.2 The Physical Meaning of Q_a

171

173 174

175

176

177

178 179

180

181

182

183

184

185

186

187

188 189

190

191 192

193 194

195

196

197

198

199

200

201

202 203

204

205

206

207

In the preceding derivation, the alteration quotient, Q_a , is intentionally defined broadly, such that it could take any value. However, there are physical and geochemical limits on the range of possible values. The apparent value of Q_a determined from a regression will, at best, reflect the net result of all relevant alteration pathways acting on O₂ and CO₂, and at worst, a meaningless relationship entangling noise, analytical uncertainty, and variable net alteration.

There are minimal, if any, relevant reactions with a positive Q_a . However, this is expected for inclusions trapping variable volumes of air and ASB. Separately, non-uniform alteration (e.g. heterogeneous Q_a) can also produce an apparent Q_a that is positive. Either explanation violates the assumptions of the BCM. When $Q_a \le 0$, the chemical interpretation depends on the oxidation state and elemental abundance of the reactants (LaRowe and Van Cappellen, 2011), as well as the completeness of the reactions. When $Q_a = -1$, O_2 is fully reacted to form CO₂, corresponding to either its complete removal by oxidation of organic matter (Landis and Berner, 2018) or the respiration by trapped microorganisms (see Vreeland et al., 2000; Lowenstein et al., 2011; Schreder-Gomes et al., 2022). More reduced organic molecules produce less CO₂ per mole of O₂ consumed, yielding Q_a values below -1 (e.g., Q_a = -2 for methane oxidation). Partial oxidation (e.g. forming CO not CO₂) (Landis and Berner, 2018) or the oxidation of non-carbonaceous compounds may produce even lower values (e.g., Q_a approaches ∞). Conversely, values between -1 and 0 may result from the oxidation of compounds containing more oxygen, or entirely anaerobic reactions.

The value of Q_a for O_2 and CO_2 holds geochemical meaning because the two gases are chemically linked (i.e. they share elemental similarities). However, when these criteria are not met, physical meaning is limited or absent entirely. There is no reaction that consumes O₂ to produce CH₄, or vice versa, as implied by OMG (Blamey and Brand, 2019; Brand et al., 2021). Such relationships would require O₂ to reduce carbon, contradicting its role as a terminal electron acceptor (LaRowe and Van Cappellen, 2011), and they could not be linear, as a third intermediate molecule, typically CO₂, is necessary. Strong negative correlations between O₂ and CH₄ may reflect mixing with secondary hydrocarbon-rich fluids or the bulk decrepitation of atmosphere rich inclusions and those containing substantial amounts of degraded organic matter. The latter may indicate prolonged heating. Secondary inclusions cannot meaningfully be included in the BCM, as they may capture multiple generations of fluids with distinct

compositions. Similarly, primary inclusions subjected to prolonged or intense heating may lose their atmospheric signatures due to physical, not chemical, alteration.

208

209

210

211

212

213214

215

216

217218

219

220

221

222

223

224

225

226

227

228

229230

231

232233

234

This conceptual inconsistency draws into question previous results obtained from applying regressions to O₂ vs. OMG (defined as CO₂ + CH₄) for halite inclusion gases. There isn't a meaningful interpretation of Q_a when defined as $\Delta O_2/\Delta OMG$, suggesting this approach rests on limited geochemical justification. Gases from modern halite inclusions contain very little CH₄ (Blamey and Brand, 2019; Brand et al., 2021; Park and Schaller, 2025). Regressions between O₂ vs. OMG and O₂ vs. CO₂ are nearly identical, but they differ greatly from O₂ vs. CH₄ (Fig. 2). This demonstrates that CH₄ is of little utility to the method. Yet many studies use O₂ vs. OMG regressions to identify ancient atmospheric oxygen contents (Blamey and Brand, 2019; Brand et al., 2021; Davis, 2018; Shaver, 2018). Greater error is introduced for inclusions containing more methane. For example, halite from the Ara group (ca. 542 Ma.) of Oman contains up to 80% CH₄ (Brand et al., 2021). Regressions of O₂ vs. OMG and O₂ vs. CH₄ yield intercepts of 19.8% and 18.7% respectively, whereas an O₂ vs. CO₂ regression has an intercept of 15.3% O₂. All three yield Q_a values near 0, implying CH₄ and CO₂ are being added without altering O₂. This is very likely evidence for the entrapment of secondary fluids containing little or no O₂. Indeed, previous studies demonstrated the Ara halite is variably impregnated with hydrocarbons, including solid bitumen, derived from the oil reserves of the underlying lithologies (Schoenherr et al., 2007), thus implying these samples are likely unsuitable for paleo atmospheric reconstruction.

The incorporation of both CO_2 and CH_4 in a BCM regression can mask two antagonistic relationships as one: O_2 and CH_4 being consumed proportionally (a positive Q_a) and O_2 and CO_2 being negatively correlated (a negative Q_a). CO_2 and CH_4 themselves may be positively or negatively correlated. These complexities indicate that the chemical relationships between the three gases cannot be described by a simple line. Inappropriately combining multiple gases on either axis may improve the fit of a regression, as variance is reduced when the sum of their relative proportions approaches 100%.

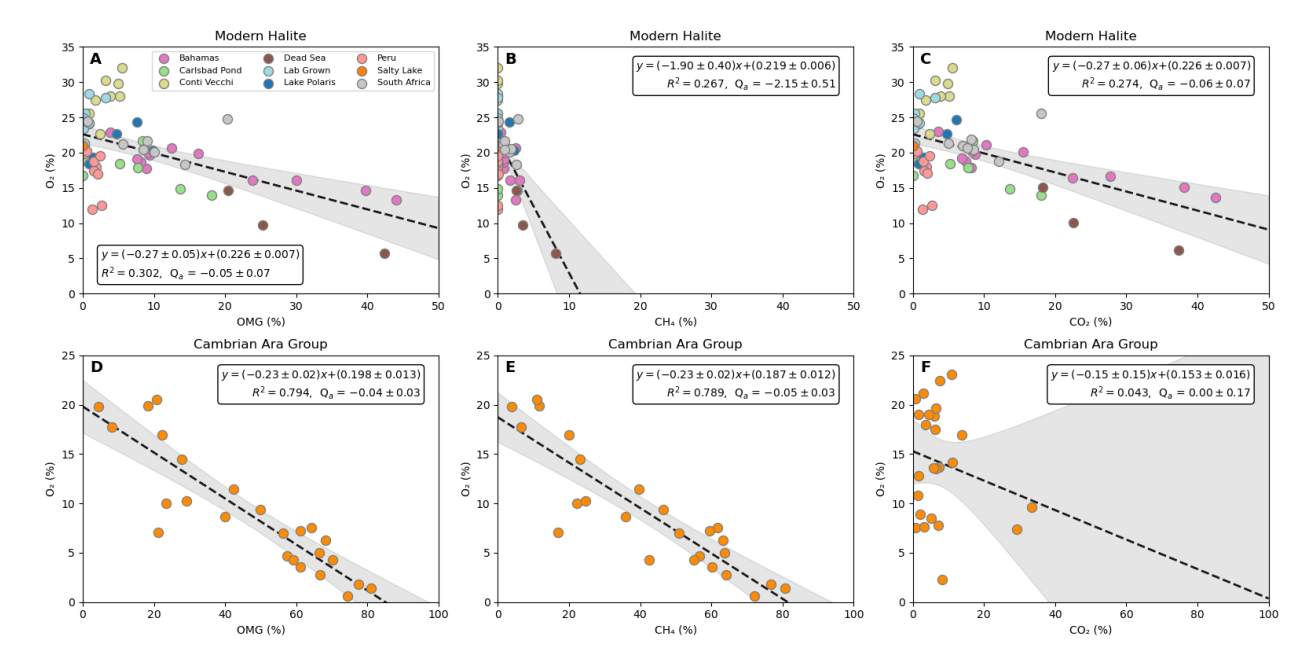


Figure 2: The back calculation method is applied to gases released from modern (A-C) and Cambrian aged (D-F) halite inclusions. O₂ vs. OMG and O₂ vs. CO₂ regressions are effectively identical for the modern halite samples, but are substantially different for the Ara halite. O₂ vs. CH₄ regressions show the opposite trend. All mole fractions are renormalized to include only N₂, O₂, Ar, CO₂, and CH₄ for the O₂ vs. OMG and O₂ vs. CH₄ plots, and just N₂, O₂, Ar, and CO₂ for the O₂-CO₂ plots. All data is sourced from (Blamey and Brand, 2019; Brand et al., 2021; Park and Schaller, 2025)

3.3 Error is Introduced when the BCM assumptions are not upheld

When the core assumptions of the BCM are not held, significant interpretive errors may be introduced. In the BCM it assumed that the intercept of the regression line reflects the O₂ contents as they were originally trapped. This is correct only when the regression has a slope of zero, or if no CO₂ was trapped. The first case renders the BCM moot, as the intercept simply reflects the unweighted average of the O₂ content. The second has more meaningful implications: if any CO₂ was trapped within the inclusion, the intercept systematically overestimates or underestimates the unaltered O₂ contents. This issue is obscured for modern halite that formed in equilibrium with negligible atmospheric CO₂ (~ 400 ppm (NOAA, 2024)), but it may be relevant for ancient samples. During the Phanerozoic, atmospheric *p*CO₂ likely never exceeded 5000 ppm (Steinthorsdottir et al., 2025; The Cenozoic CO2 Proxy Integration Project (CENCO2PIP) Consortium, 2023). However, fully aqueous inclusions could reasonably contain a few 10s of percent of CO₂ because of the comparatively high solubility of CO₂ relative to the other atmospheric gases (Fig. S9). Since the BCM describes how O₂ and CO₂ relate (Equation 12), the original abundance of either gas cannot be known without independent constraints on the other.

The other two assumptions implicit to the BCM are satisfied only when Q_a , X^t_{O2} , and X^t_{CO2} are identical across samples, and if the other inclusion gases occur in consistent abundances (e.g. constant N_2/Ar). There is evidence these assumptions are not held for gases

contained by many modern halite samples. First, there are distinct regressions between localities (Fig. 3, Table 1), which highlights the inappropriateness of applying a single BCM across different localities, as has been done previously (Blamey and Brand, 2019; Brand et al., 2021). Half of the regressions yield positive apparent Q_a values that are unlikely to be caused by uniform alteration, and another two yield values near zero. Despite this, the intercepts are in general agreement with modern atmospheric O_2 levels (e.g., 21%), with values ranging from 18.8 % to 23.9% O_2 with uncertainties between ± 0.6 to ± 4.4 %. This is fitting with the expectation of the BCM, as the least altered (e.g., most atmospheric) samples will exert greater direct influence on the intercept. However, there are factors that warrant additional consideration.

 A deviation of \pm 2-3% may seem small relative to the modern atmosphere, but it could represent a substantial relative error for samples precipitating under an atmosphere with much less O₂. The R² of the regressions vary from 0.01 to 0.87. The weaker fits suggest inconsistent relationships between O₂ and CO₂, possibly reflecting noise, outliers with disproportionate influence, or multiple relationships within the data (e.g., variable Q_a , non-uniform initial compositions, or alteration involving other inclusion gases). For these relationships the residuals are inconsistent (Fig. S10). When highly influential points (i.e. those with large Cook's distances) are removed, R² values improve, sometimes substantially (e.g., see Lake Polaris and South Africa, Fig. S11). At the same time the intercepts appear less atmospheric, ranging from 17.5 % to 24.3 % O₂, and some Q_a values are completely changed. Conversely, the regression with the highest R² (i.e., the Dead Sea halite) contains just three data points, making it far more susceptible to outliers, noise, and any data point with significantly more or less CO₂, as implied by the large 95% confidence interval. *This begs the question, are these intercepts simply fortuitous?* More broadly, *can other properties of the fluids help explain the variance?*

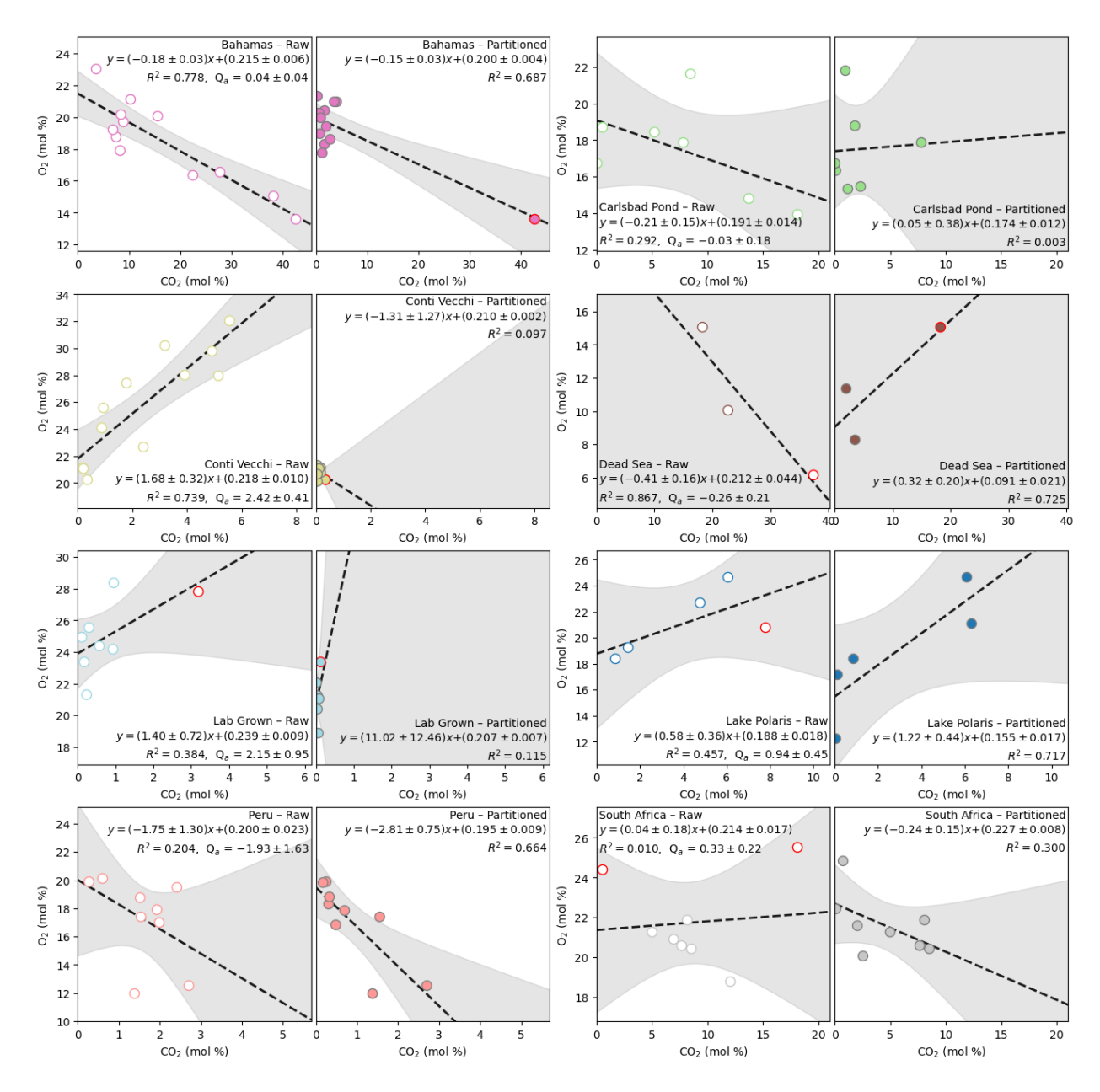


Figure 3: The BCM is applied to the raw (left side of each pair) and partitioned (right side) gas compositions from modern halite inclusions. Each pair of plots represents one locality. Regressions are distinct between localities. Datapoints outlined in red have a Cook's distance exceeding 1, indicating a strong influence on the regression. All data is sourced from (Blamey and Brand, 2019; Brand et al., 2021; Park and Schaller, 2025)

3.4 Alteration is not the only source of molecular compositional variability

There are numerous reasons to expect compositional variability between inclusions, even among those formed within similar depositional environments. For example, halite can precipitate at the air-water interface or the sediment-brine interface (Roedder, 1984b), where trapped gas compositions may differ based on the distinct chemical conditions prevailing at each

depth. Other physical effects, such as diffusion, may also introduce heterogeneity, as is the case for soil carbonates precipitated at various depths (Cerling, 1995). Broadly speaking, alteration may occur prior to fluid entrapment. Water bodies that are out of equilibrium with the atmosphere may contain gas excesses or deficits dictated by biogeochemical processes occurring in the water column. Take for example the Dead Sea: due to a variety of physicochemical processes the brines contain very low dissolved oxygen levels (Shatkay et al., 1993) and elevated CO₂ contents (Golan et al., 2017). Gases released from Dead Sea halite show the same effects (Figure 3). Inclusions trapping variable volumes of atmosphere and this out of equilibrium brine may yield similar compositions to those that have been altered post entrapment, yet they may require unique corrections (Fig. S12).

 A major, and often overlooked, source of variability is physical chemistry. Inclusions forming at or near the air-water interface capture variable volumes of the two phases, which, due to the unique solubility of each gas, contributes to significant compositional variability (Park and Schaller, 2025; Pettitt et al., 2020; Yeung, 2017). Inclusions are unlikely to trap the same gas composition, unless they form under the same physicochemical conditions with the same φ_g . Since O_2 and CO_2 have increased solubilities relative to N_2 (Sander, 2023), the most abundant atmospheric gas, Q_a will appear positive for unaltered inclusions of variable φ_g . (e.g, See Conti Vecchi halite in Fig. 3).

The combined effects of physical chemistry and post entrapment alteration can produce a very large range of possible gas compositions (Fig. 4), as seen with the modern inclusion data. It is possible that the extent of alteration and the alteration pathway may vary with φ_g . Phase chemistry greatly expands the space of possible regressions, and provides a clear explanation for why regressions may not pass through the atmospheric condition. Previous assertions regarding the BCM, that "any population should be able to resolve a global atmospheric oxygen value." (Brand et al., 2021, pg. 8), are simply untrue. To accurately interpret BCM regressions, phase chemistry must be accounted for.

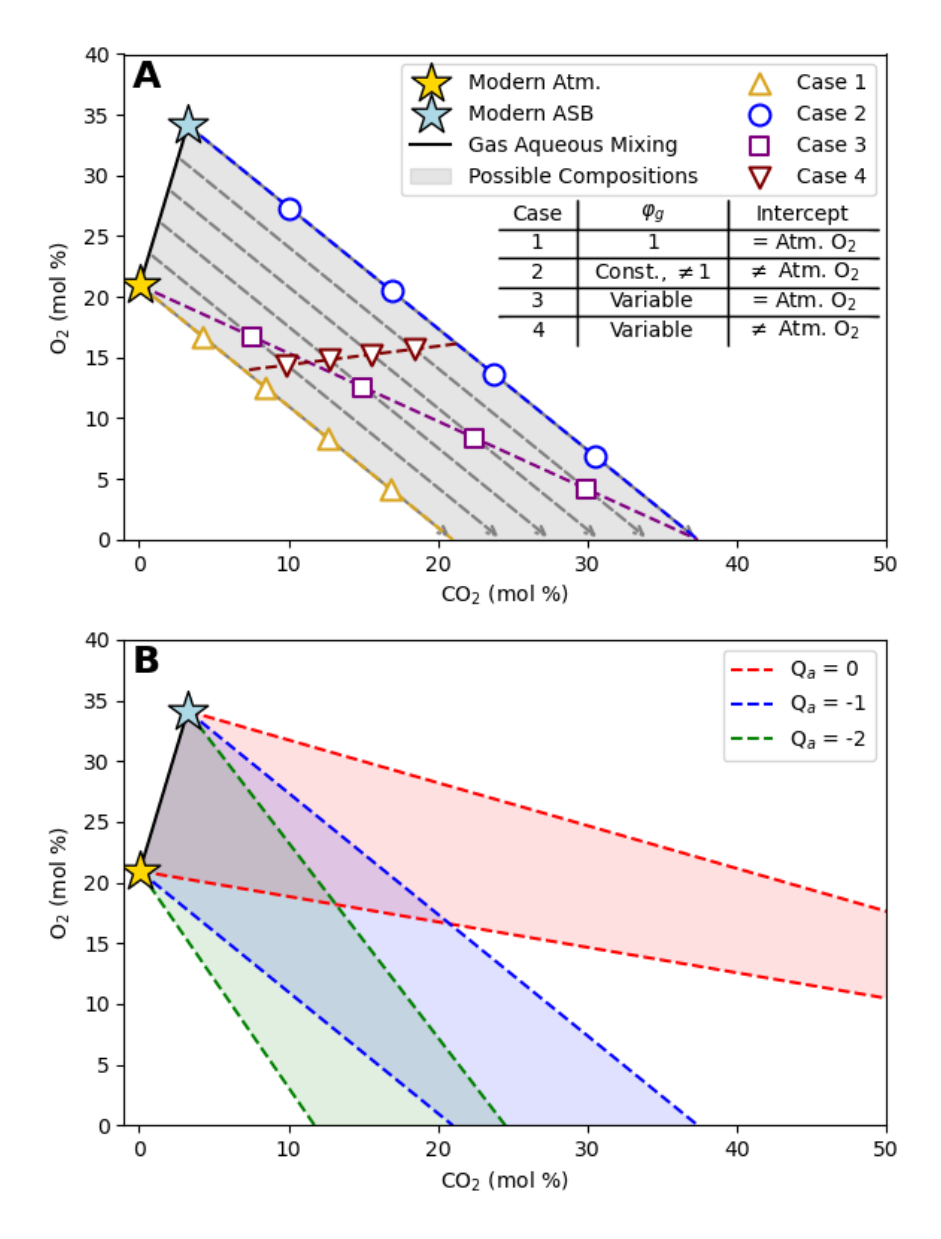


Figure 4: Both physical chemistry and alteration introduce variability in the amount of O_2 and CO_2 released from fluid inclusions. The relative abundance of the two gases increases as inclusions trap less atmosphere (gold stars) and more brine (blue stars). A) A range of compositions is possible when Q_a is constant (filled grey area, e.g., Q_a = -1). Four types of BCM regressions are possible within this range. Fully gaseous inclusions (φ_g = constant = 1) will yield intercepts that match atmospheric O_2 values (assuming negligible CO_2 , Case 1). Inclusions that trap a consistent mix of air and brine (φ_g = constant < 1) will not (Case 2). Depending on alteration extents, variable φ_g may or may not yield atmosphere-like intercepts (Case 3 and 4). B) The breadth of possible compositions increases if multiple alteration pathways are considered (i.e. distinct Q_a). Individual compositions can be obtained from multiple pathways. Models are calculated for modern atmosphere and 7.5 M NaCl brines trapped at 25 °C.

It is possible to use the ratios of conservative gases not included in the BCM (e.g., N_2/Ar) to check for the possibility of gas-aqueous mixing (Park and Schaller, 2025). From equation 2 it follows that the ratio of any two gases as initially trapped within an inclusion can be expressed as:

$$\frac{n_i^t}{n_j^t} = \frac{P_i Y_i \left(\varphi_g, T, S\right)}{P_j Y_j \left(\varphi_g, T, S\right)} = \beta_{i-j} \left(\varphi_g, T, S\right) \frac{P_i}{P_j}$$
Eq. 17

where β_{i-j} is a specific partition coefficient reflecting the relative solubility of the two gases (Note: previously α_{i-j} has been used to denote this quantity, β_{i-j} is used here to avoid confusion with the isotopic fractionation factor used below). If the observed gas ratios vary beyond analytical uncertainty, then they either represent entrapment with variable φ_g , or alteration of species assumed to be conservative. Both scenarios violate the core assumptions of the BCM. Further, any two gas ratios should be related by a parametric curve as a function of φ_g . Modern halite inclusions show variability that in part can be explained by mixing of variable volumes of air and ASB (Fig. 5) (Blamey and Brand, 2019; Brand et al., 2021; Park and Schaller, 2025).

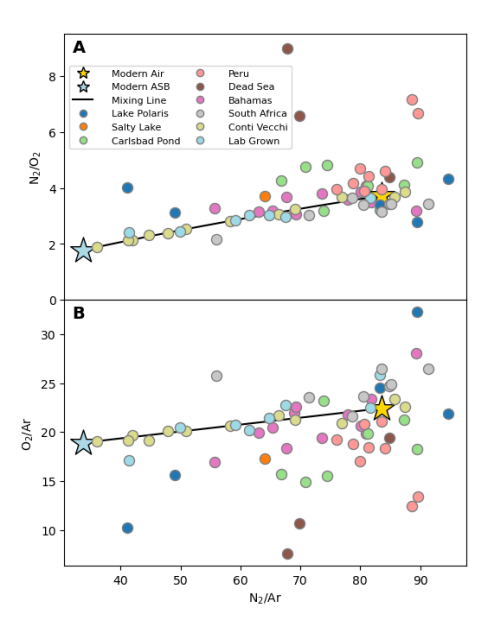


Figure 5: A) N₂/O₂ and B) O₂/Ar ratios are compared against N₂/Ar ratios for modern halite inclusion gases. Variability can partially be explained by the mixing of trapped atmosphere (gold stars) and air saturated brine (blue stars). Datapoints that don't fall along predicted mixing models (black lines) are likely altered to greater extents. Modeled curves assume 25 °C and 7.5 M NaCl inclusion fluids. All data is sourced from (Blamey and Brand, 2019; Brand et al., 2021; Park and Schaller, 2025)

3.5 Accounting for Phase Chemistry

A simple way to account for the effects of phase chemistry is to bin the data based on φ_g and fit separate regressions for each bin. If Q_a is constant within a bin, the regression should pass through the unaltered trapped composition. However, only inclusions dominated by air will pass through the atmospheric composition.

 φ_g can be inferred from $\beta_{\text{N2-Ar}}$ if the atmospheric N₂/Ar ratio is known. For the modern atmosphere this ratio is approximately 84. Reasonable constraints on ancient N₂/Ar ratios can be placed based on the ratios observed within inclusions (Park and Schaller, 2025) and plausible estimates from models and proxies. Like the BCM, this method of calculating φ_g implicitly assumes the conservative gases have not been altered. If there is abundant ⁴⁰Ar ingrowth, another set of appropriately conservative gases can be used. In principle, $\beta_{\text{N2-Ar}}$ should not exceed 1, yet values above 1 are frequently observed in modern halite data. These inclusions are assumed to be fully gaseous, which introduces a confounding source of error.

Applying a binary binning to gas data from the Bahamas halite demonstrates this effect (Fig. 6). A regression through the most gaseous points yields an intercept matching atmospheric O₂ levels, whereas the more aqueous points yield an intercept farther from atmospheric, but consistent with predicted O₂ levels for that mix of gas and brine. Even though these fits are stronger than the original, the binning is largely arbitrary. In theory, increasing the number of bins could produce stronger relationships. However, the statistical robustness of the regression tends to decrease with fewer points. At the extreme, isolating each datapoint makes it impossible to use a regression.

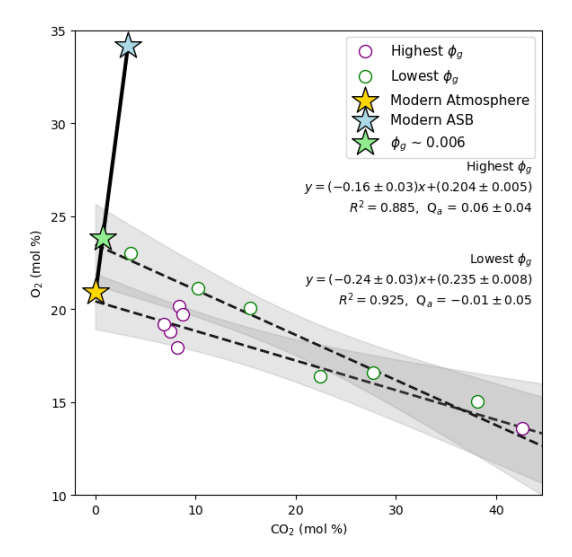


Figure 6: Mole fractions of O_2 and CO_2 are compared for modern halite from the Bahamas (Blamey and Brand, 2019; Brand et al., 2021). The data is arbitrarily split into two bins based on φ_g values. A regression fit to the data with the highest φ_g (avg. = 0.201, range = 0.012–1) produce a nearly atmospheric intercept. A regression fit to the bottom six points (avg. = 0.006, range = 0.002-0.008) yields an intercept closely matching the value expected for inclusions with φ_g = 0.006. Both regressions have stronger R^2 compared to a regression through all of the data.

To improve upon this, the data can be partitioned and corrected. Park and Schaller (2025) developed the program MAGPI (Method for Atmospheric Gas Partitioning from fluid Inclusions) to partition inclusion data based on observed N₂/Ar ratios and apply a unique correction to each sample. The magnitude of the correction is dependent on how gaseous the sample is perceived to be. The correction effectively inverts equation 1 and computes new partitioned mole fractions for each gas:

$$X_{i}^{p} = \frac{\frac{n_{i}^{t} + \Delta n_{i}}{Y_{i}\left(\varphi_{g}, T, S\right)}}{\sum_{j \in J} \frac{n_{j}^{t} + \Delta n_{j}}{Y_{j}\left(\varphi_{g}, T, S\right)}}$$
Eq. 18

Here X_i^p reflects the partitioned atmospheric composition the inclusions are perceived to have formed under. If no alteration has occurred, this is equal to the true atmospheric composition (X_i^{atm}) . The relationship between $X_{O_2}^p$ and $X_{CO_2}^p$ is derived in the same manner as equation 11 (Supporting Information) and takes a similar form:

$$X_{O_2}^p = \frac{X_{CO_2}^p \left[X_{O_2}^{atm}(k+1) - k \right] + \left[X_{CO_2}^{atm}k - X_{O_2}^{atm} \right]}{X_{CO_2}^{atm}(k+1) - 1}$$
 Eq. 19

392 Where

$$k = \beta_{CO_2 - O_2} Q_a$$
 Eq. 20

 This presents a linear relationship if k is constant between points. This represents a major improvement, in that regressions satisfying this constraint will pass through the true atmospheric composition ($X_{O_2}^{atm}$ and $X_{CO_2}^{atm}$). In other words, the point at which these regressions intersect is the atmospheric composition (Figs. S13-S15). This also implies the least altered gases will cluster around the atmospheric composition when partitioned. This was previously shown for the Conti Vecchi and Lab Grown halite, whose gas compositions collapse to match that of the modern atmosphere when partitioned (Park and Schaller, 2025) (Fig. 3).

It is important to note that we are not implying that partitioning altered gas data will automatically yield true atmospheric compositions. When applying this method to the other modern halite gases, some converge toward atmospheric values (e.g., the Bahamas halite), while others remain scattered about non-atmospheric compositions (Fig. 3, Table 1). Greater scatter likely reflects a combination of variable φ_g and Q_a values. For regressions through corrected data with constant φ_g , an apparent Q_a can be calculated similar to equation 16:

$$Q_a = \frac{m^p + b^p}{\alpha_{CO_2 - O_2}(1 - b^p)}$$
 Eq. 21

408

409 410

411

 Q_a can also be estimated individually with specific delta values for O_2 and CO_2 . The expected moles of either gas can be calculated relative to the observed moles of N_2 by inverting the partitioning (Park and Schaller, 2025). The difference between the observed moles of each gas and this value is the change in moles:

$$\Delta n_i = n_i^{obs} - \frac{X_i^{ref}}{X_{N_2}^{ref}} \left(\frac{n_{N_2}^{obs}}{\beta_{N_2 - i}(\varphi_g, T, S)} \right)$$
 Eq. 22

Where β_{N_2-i} is the relevant partition coefficient between N_2 and either O_2 or CO_2 , and X_i^{ref} are 412 reference mole fractions. If atmospheric compositions are known, they can be referenced to 413 414 calculate exact Δ values, assuming the conservative species are observed at their expected abundances. For the modern halite inclusions, this allows us to examine exactly how alteration 415 416 has affected the trapped gases. The extent of alteration varies between the two gases for each sample, and thus distinct Q_a values are observed. Some localities yield narrower ranges of Q_a 417 418 than others, which supports the dominance of one alteration pathway. The degree to which 419 individual Q_a values agree with values estimated from unpartitioned regressions varies across 420 sites (Fig. 7, Table 1).

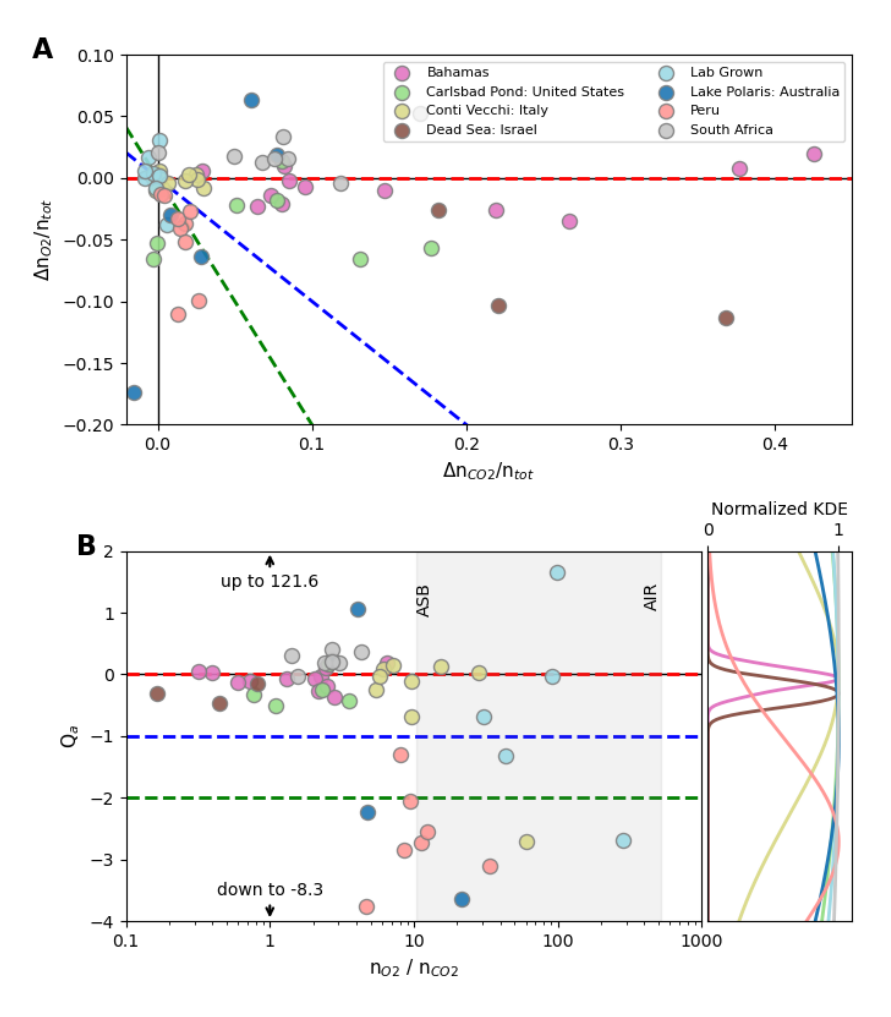


Figure 7: A) Normalized Δ values are compared for O_2 and CO_2 released from modern halite inclusion. Radial dashed lines represent lines of equal Q_a (red = 0, blue = -1, and green = -2). Points closer to the origin tend are less altered. B) Individual Q_a values are plot against observed O_2/CO_2 ratios to show their deviance from the range expected from gas-aqueous equilibrium. Normalized kernal density estimates (KDEs) are shown. The y axes are trimmed to highlight the datasets that cluster about $Q_a = 0$. Δ values are calculated from equation 22 using the modern atmospheric composition as reference and assuming 25 °C and a 7.5 M NaCl equivalent salinity within the inclusions.

Table 1: Alteration quotients and partitioned gas compositions are compared across modern halite localities. Q_a values determined from BCM regressions are compared to actual values determined using equation 22. The closed geometric means of the partitioned compositions (Aitchison center) are presented with 95% confidence intervals, quantified using a non-parametric bootstrap (10,000 resamples with replacement). Partitioning was performed with the program MAGPI (Park and Schaller, 2025), assuming 25 °C and a 7.5 M NaCl equivalent brine.

	Locality (Refs.)	Avg. Q_a (BCM)	Actual Q _a	Partitioned Gas Composition (%, 95% CI)	pO ₂ (mbar)	pCO ₂ (ppm)	
--	------------------	------------------	-----------------------	---	------------------------	------------------------	--

		(Med, Min, Max)	N_2	O_2	Ar	CO_2		
Bahamas (Blamey and Brand, 2019; Brand et al., 2021)	0.04 ± 0.04	-0.07, -0.36, 0.20	77.3 ^{+1.2} _{-2.5}	20.0+0.7	$0.92^{+0.02}_{-0.04}$	1.82 ^{+2.42} _{-0.91}	202+11	18000+24000
Carlsbad Pond (Blamey and Brand, 2019; Brand et al., 2021)	-0.03 ± 0.18	-0.23, -0.50, 121.6	80.8 ^{+1.5} _{-2.7}	17.7 ^{+1.7} _{-1.5}	0.95 ^{+0.03} _{-0.04}	$0.56^{+2.14}_{-0.45}$	171+21	5400+21000 -4300
Conti Vecchi (Park and Schaller, 2025)	2.42 ± 0.41	0.06, -2.72, 10.0	78.2 ^{+0.2} _{-0.2}	$20.8^{+0.2}_{-0.2}$	$0.93^{+0.03}_{-0.03}$	$0.08^{+0.04}_{-0.02}$	208+2	770+380 -250
Dead Sea (Blamey and Brand, 2019; Brand et al., 2021)	-0.26 ± 0.21	-0.31, -0.47, - 0.14	82.2 ^{+5.1} _{-16.3}	$11.7^{+3.4}_{-3.4}$	0.98 ^{+0.07} _{-0.20}	5.2 ^{+13.1} _{-3.2}	111+67	49000+167000
Lab Grown (Park and Schaller, 2025)	2.15 ± 0.95	-0.35, -6.48, 30.6	77.9+0.9	21.1+0.9	0.93 ^{+0.01} _{-0.01}	0.03 ^{+0.03} _{-0.02}	212+11	300+280 -150
Lake Polaris (Blamey and Brand, 2019; Brand et al., 2021)	0.94 ± 0.45	0.24, -3.65, 10.9	79.7+4.3	18.8+3.8 -3.9	0.92 ^{+0.08} _{-0.09}	$0.62^{+3.60}_{-0.53}$	184+53	6100+39000
Peru (Blamey and Brand, 2019; Brand et al., 2021)	-1.93 ± 1.63	-2.85, -8.31, - 1.31	81.5 ^{+1.6} _{-1.5}	16.9+1.7	0.96 ^{+0.01} _{-0.01}	$0.58^{+0.46}_{-0.24}$	162+20	5600+4300
Salty Lake (Blamey and Brand, 2019; Brand et al., 2021)			81.2	17.9	0.97	~0	172	2
South Africa (Blamey and Brand, 2019; Brand et al., 2021)	0.33 ± 0.22	0.26, -0.03, 68.0	74.9 ^{+1.4} _{-2.9}	22.1 ^{+0.9} _{-1.2}	$0.88^{+0.02}_{-0.04}$	2.15+3.58	231+11	22000+40000 -16000
Modern Atmosphere (Brimblecombe, 1996; NOAA, 2024)			78.08	20.95	0.93	~0.04	209.5	~400

In determining ancient atmospheric compositions, the geometric mean of the partitioned gas ratios can be referenced to evaluate each points displacement relative to the central composition. In this case, the equation shows the change in moles necessary to obtain a uniform composition. Some caution is necessary, as this composition is not necessarily atmospheric (e.g., centered about an altered composition). Incorporating other observables (e.g., whether observed gas ratios fall along a parametric line) can help examine the efficacy of partitioning. A plot of Δn_{O_2} vs. Δn_{CO_2} can inform whether there are trends in the data. Relative deviations can be determined by normalizing to the moles of either gas or the total moles observed. If the data falls along a line passing through the origin, a larger trend persists in the data. That line defines an apparent Q_a that the samples share that has not been accounted for fully.

3.6 Isotope Ratio Measurements of Inclusion CO₂

The preceding discussion highlights the modifications necessary to determine atmospheric gas compositions using the BCM. In many instances, simply estimating Q_a is insufficient to correct for the effects of alteration, particularly for ancient samples with unknown atmospheric contents. Isotope ratios can provide additional information to solve this problem. The initial isotope ratio of gases trapped within an inclusion (R_t) reflects the mixing of variable volumes of air and ASB (Park and Schaller, 2025).

$$R_t = \frac{R_{atm}n_{gas} + R_{brine}n_{aq}}{n_{gas} + n_{aq}}$$
 Eq. 23

Assuming equilibrium was reached between the two phases prior to entrapment, the isotope ratios of the two phases can be linked by specific equilibrium fractionation factors (α_{g-aq}). Thus R_t can be determined from the atmospheric ratio following:

$$R_t = R_{atm} \left(\frac{\frac{\varphi_g}{RT} + \alpha_{g-aq} (1 - \varphi_g) H_s}{\frac{\varphi_g}{RT} + (1 - \varphi_g) H_s} \right)$$
 Eq. 24

457 If a gas had not reached equilibrium, the trapped ratios may not be proportional to those of the atmosphere and more general mixing models would be necessary. Alteration may further 458 459 fractionate the trapped gases. In such cases a hierarchical mixing model is necessary to deconvolute the various isotopic effects. Since CO₂ is in excess for many modern halite gases, 460 the observed $^{13}\text{C}/^{12}\text{C}$ ratio (R_{obs}) could be useful in identifying the degree of alteration. The 461 462 requisite mathematical treatment of this data depends on the type of alteration. Alteration that adds CO_2 introduces carbon with a distinct isotope ratio (R_{alt}) that can shift the bulk ratio of the 463 inclusion CO₂. The fraction of CO₂ that was originally trapped in the inclusion (f_t) can be 464 465 calculated from mass balance assuming:

$$f_t = \frac{R_{obs}^{13C} - R_{alt}^{13C}}{R_t^{13C} - R_{alt}^{13C}} = \frac{n_{CO_2}^t}{n_{CO_2}^t + \Delta n_{CO_2}}$$
 Eq. 25

Alteration that removes CO₂ may preferentially consume one isotope progressively enriching the remaining CO₂ in the other (i.e. a negative Δn_{CO_2} with fractionation α_{alt}). The fraction of CO₂ remaining in the inclusion (f_r) can be determined via a Rayleigh-type fractionation model:

$$f_r = \left(\frac{R_{obs}}{R_t}\right)^{\frac{1}{\alpha_{alt}-1}} = \frac{n_{CO_2}^t + \Delta n_{CO_2}}{n_{CO_2}^t}$$
 Eq. 26

From both equations, Δn_{CO_2} can be calculated assuming R_{atm} , φ_g , and either R_{alt} or α_{alt} are known. 469 If Q_a is known the relevant alteration of CO₂ and O₂ can be addressed to provide a more accurate 470 471 estimate of the atmospheric composition. 472 Empirically constraining R_{atm} values may be difficult, however, estimates can be garnered from 473 established records of marine carbonates and buried organic matter. Apart from a few major excursions, these records reveal fairly consistent carbon isotope ratios through time (Garcia et 474 475 al., 2021), which suggests atmospheric ratios may be similar to preindustrial values, typically -6‰ to -8‰ (VPDB, $R_{atm} \approx 0.011170 - 0.011147$) (Rubino et al., 2013). If R_{obs} is close to or 476 477 within this range, the samples likely have experienced minimal alteration and are more representative of the atmosphere. Thus, it is possible to constrain R_{atm} directly with the most 478

- 479 pristine samples. Values that are further away reflect greater alteration. R_{alt} likely reflects CO_2
- introduced biogenically or through organic matter decomposition with values between -25‰ and
- 481 -30% ($R_{alt} \approx 0.010956 0.010900$) (Garcia et al., 2021). Alternatively, these values can be
- 482 estimated relative to R_{atm} using appropriate fractionation factors (e.g. the nominal fractionation
- 483 associated with RuBisCO is $\varepsilon \approx -20\% = 1000(\alpha_{alt} 1)$; Farquhar et al., 1989).
- As proof of concept, we measured the δ^{13} C of CO₂ released from several halite samples using an
- 485 Isoprime 100 Dual Inlet Isotope Ratio Mass Spectrometer at RPI (Supporting Information, Table
- 486 S1). While the φ_g of the samples is unknown, an apparent range of f_t values can be estimated
- 487 (Fig. 8). For these calculations $\delta^{13}C_{atm}$ values were obtained from modern and glacial ice core
- 488 records and extrapolated from ancient marine carbonates (Supporting Information). $\delta^{13}C_{alt}$ was
- assumed to be -20% lighter than $\delta^{13}C_{atm}$. Notably, halite from the 1.44 Ga. Sibley group yielded
- 490 a δ^{13} C of -8.38 \pm 0.20% (Park et al., Accepted), indistinguishable from estimated atmospheric
- values (0.97 < f_t < 1.0). This observation supports the authenticity of the 2760 \pm 1660 ppm CO₂
- obtained from the same samples (Park et al., Accepted). In contrast, halite from Death Valley
- 493 (collected in 1994), Baja California (collected in 1980), and the Atacama Desert (69 Ka) yield
- much lower δ^{13} C values (-20.09 ± 0.15% to 25.60 ± 0.34%). While their bulk CO₂ abundances
- 495 were not measured, these measurements indicate the dominance of alteration-derived carbon (f_t <
- 496 0.34). Finally, CO₂ from a sample of Conti Vecchi halite (collected in 2012) yielded an
- intermediate ratio of δ^{13} C = -15.56 ± 1.61% (Supporting Information), which suggests a
- balanced mixture of atmospheric and altered carbon (0.55 $\leq f_t \leq$ 0.76). Applying these values to
- the bulk CO₂ recorded by the Conti Vecchi halite (770⁺³⁸⁰₋₂₅₀ ppm, Table 1) yields between
- $500 \qquad 490^{+330}_{-200} \text{ ppm (assuming } \phi_g=1, \text{ fully gaseous) and } 520^{+350}_{-210} \text{ ppm (assuming } \phi_g=0, \text{ fully gaseous)}$
- aqueous). These values overlap and more strongly agree with recorded atmospheric CO₂ (~393
- ppm in 2012, (NOAA, 2024)). The accuracy of these results could be improved by measuring the
- δ^{13} C of trapped organic matter directly. Inverting the mass balance, we find a δ^{13} C_{alt} of -23.2% to
- -22.0% would reproduce the observed atmospheric CO₂ (Fig. S16).

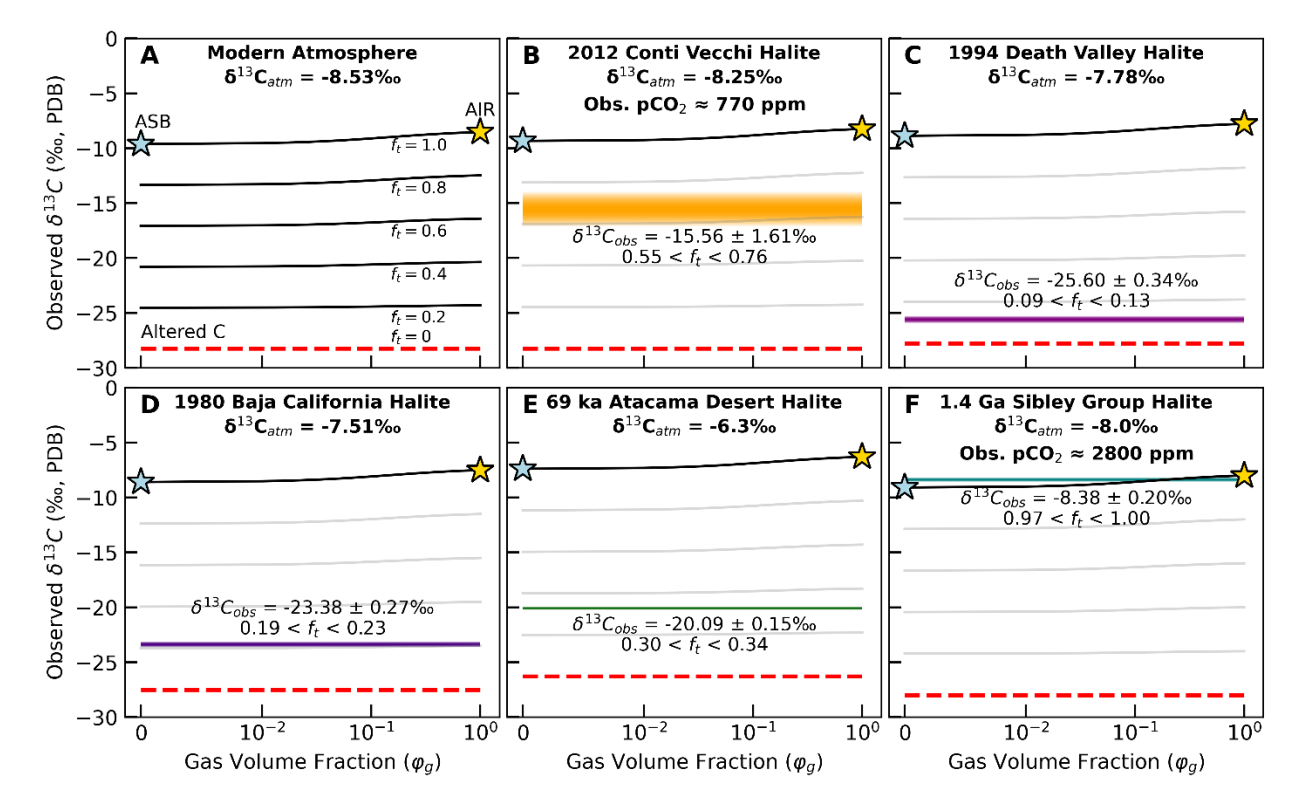


Figure 8: The δ^{13} C of CO₂ trapped within an inclusion reflects the relative mixing of trapped air (δ^{13} C_{atm}, gold stars) and ASB (blue stars). Alteration may add CO₂ with a distinct carbon isotope ratio (δ^{13} C_{alt}, red dashed lines). The unaltered fraction of inclusion CO₂ (f_t) can be determined through mass balance if the δ^{13} C is measured and δ^{13} C_{atm}, δ^{13} C_{alt}, and φ_g are known (Equations 24 and 25). A) An example mass balance for modern fluid inclusions shows lines of equal alteration (constant f_t , black lines) for variable φ_g . Observed δ^{13} C values from modern (B-D) and ancient (E, F) halite inclusion CO₂ (δ^{13} C_{obs}, colored bars) are distinct and reveal variable degrees of alteration. All calculations assume inclusions formed at 25 °C with a 7.5 M NaCl equivalent salinity, and that alteration introduces CO₂ with δ^{13} C_{alt} = δ^{13} C_{atm} - 20‰. δ^{13} C_{atm} values are from the Isotopic Data Gallery from the Scripps CO₂ Program (https://scrippsco2.ucsd.edu/), glacial ice records (Eggleston et al., 2016), and extrapolated from marine carbonates (Krissansen-Totton et al., 2015) using standard equilibrium fractionations (Deines et al., 1974; Zhang et al., 1995).

3.7 Application to Ancient Samples: A Path Forward

The preceding discussion outlines several limitations of applying the BCM in its original form to determine atmospheric compositions from fluid inclusions. As a result, the method is applicable to only gas dominated inclusions (i.e., high and consistent φ_g), where alteration has uniformly influenced exclusively O₂ and CO₂. Applying the BCM to unpartitioned data is often insufficient to properly address all sources contributing to compositional variability. Further, this technique emphasizes the importance of O₂ over CO₂ (Blamey and Brand, 2019; Brand et al.,

2021), despite a demonstrated utility of inclusions for constraining atmospheric CO₂ levels (Park and Schaller, 2025; Hudgins et al., In Review). Partitioning the gas from aqueous phase expands the range of valid datasets, such that regressions pass through the atmospheric composition if φ_g and Q_a values are consistent. This modification allows both O₂ and CO₂ levels to be found, within error, by identifying the intersection of regressions through two or more appropriately constrained subsets of the data. For both raw and partitioned data, the strength of a linear regressions can serve as a crude but useful test of a dataset's validity: low R² values may indicate variable alteration or heterogeneous φ_g .

For ancient samples, it is important to distinguish between primary, secondary, and altered inclusions. Screening protocols emphasize the steps necessary to separate primary and secondary samples (Blamey and Brand, 2019); however, primary inclusions often retain signatures of alteration. Successfully separating the three populations is critical to properly interpreting the inclusion gases. While there is currently no protocol to identify the extent of gas alteration prior to analysis, there are methods that can reduce the likelihood of incorporating heavily altered inclusions. A variety of petrographic techniques have been used to identify microorganisms and organic matter trapped within inclusions (see Vreeland et al., 2000; Lowenstein et al., 2011; Schreder-Gomes et al., 2022). Non-destructive analytical techniques, such as Raman spectroscopy (see Frezzotti et al., 2012; Osterrothová and Jehlička, 2011; Winters et al., 2013), provide complementary information relevant to characterizing the trapped material and gases. If possible, secondary and heavily altered inclusions should also be analyzed for their gas contents. Their compositions, while not necessarily atmospheric, provide end members to which the primary samples should be compared. Statistical evaluations of the three populations can assess the degree of mixing. If altered inclusions can be identified prior to analysis, the BCM may be better suited as a diagnostic tool to examine the reactions that have altered inclusion gases. The different means for estimating Q_a presented here should be incorporated and compared.

As described above, isotope ratio measurements should be incorporated to further distinguish between atmospheric and altered inclusion gases. Beyond $\delta^{13}C$ measurements, $\delta^{15}N$ and $^{40}Ar/^{36}Ar$ ratios can be used to identify sources of alteration among the conservative gases (Blamey and Brand, 2019; Denk et al., 2017; Rama et al., 1965). For example, when β_{N2-Ar} exceeds 1 for inclusion gases, the phase relationships present within the inclusions are obfuscated. Isotopic constraints may identify sources of excess N_2 (e.g., denitrification) or Ar loss (diffusion). Ideally, compositional and isotopic measurements would be made on the same aliquots of gas.

Few records of ancient atmospheric O_2 from fluid inclusions exist have incorporated partitioning and many have utilized BCM regressions between non-compatible gases (e.g., O_2 vs. OMG). It is unclear whether these datasets meet the criteria we have defined here, and thus reevaluations are necessary to identify the relative influences of phase chemistry and alteration.

4.0 Conclusions

Gases released from fluid inclusions provide the rare opportunity to study the evolution of Earth's atmosphere directly. However, significant compositional variability among samples of similar origin can arise from both physical chemistry and post depositional alteration. Back calculation methods attempt to determine unaltered atmospheric compositions by fitting regressions to the observed O₂ and CO₂ mole fractions. Yet, they do not account for gas-aqueous equilibria and often misattribute variability to alteration alone. By deriving the mathematical framework underlying these methods, we identify and address their core assumptions and examine their limitations. We find that real datasets show evidence of non-uniform trapping conditions, as well as variable alteration acting upon the inclusion gases, all of which violate the core assumptions and limitations of the BCM.

By incorporating partitioning techniques, we provide means to account for variable gas solubilities. Stark differences are observed between alteration quotients determined through traditional back calculation methods and determined individually after accounting for phase chemistry, highlighting the error that is introduced when variability is wrongly attributed to alteration alone. A combination of the two techniques can yield true atmospheric gas compositions, but some datasets may require additional information. We show alteration can be further assessed through stable carbon isotope measurements of inclusion CO_2 . Mass balance can be used to correct the trapped CO_2 contents of heavily altered inclusion gases, whereas the least altered samples can be used to put constraints on paleo atmospheric $\delta^{13}C$.

We conclude that back calculation methods have often been implemented incorrectly in fluid inclusion-based paleo atmospheric reconstructions. The conclusions drawn from these studies should be revisited and a thorough reinterpretation of the available data is necessary. In future studies, we emphasize the importance of evaluating the extent of alteration prior to bulk gas analyses. The development of such screening protocols will greatly advance our ability to accurately characterize the trapped gases, as will incorporating improved analytical techniques that couple compositional and isotopic measurements. These improvements will improve confidence in the interpreted results, paving the way for robust direct records of atmospheric O_2 and CO_2 evolution.

Acknowledgements:

- This work was supported by National Aeronautics and Space Administration grant
- #80NSSC19M0069 and the Hamilton Endowed professorship to MFS. The authors thank Dr.
- 598 Sasha Wagner and Dr. Jacob Shelley for their insightful discussions.

References:

- 600 Aitchison, J., 1982. The Statistical Analysis of Compositional Data. J. R. Stat. Soc. Ser. B 601 Methodol. 44, 139–160. https://doi.org/10.1111/j.2517-6161.1982.tb01195.x
- Avice, G., Marty, B., Burgess, R., Hofmann, A., Philippot, P., Zahnle, K., Zakharov, D., 2018.
 Evolution of atmospheric xenon and other noble gases inferred from Archean to
 Paleoproterozoic rocks. Geochim. Cosmochim. Acta 232, 82–100.
 https://doi.org/10.1016/j.gca.2018.04.018
- Bauska, T., 2025. Ice core records of atmospheric carbon dioxide. Encycl. Quarternary Sci. 3, 122–137. https://doi.org/10.1016/B978-0-323-99931-1.00264-6
 - Berner, R.A., Landis, G.P., 1988. Gas Bubbles in Fossil Amber as Possible Indicators of the Major Gas Composition of Ancient Air. Science 239, 1406–1409.
 - Blamey, N.J.F., Brand, U., 2019. Atmospheric gas in modern and ancient halite fluid inclusions: A screening protocol. Gondwana Res. 69, 163–176. https://doi.org/10.1016/j.gr.2018.12.004
- Blamey, N.J.F., Brand, U., Parnell, J., Spear, N., Lécuyer, C., Benison, K., Meng, F., Ni, P.,
 2016. Paradigm shift in determining Neoproterozoic atmospheric oxygen. Geology
 44, 651–654. https://doi.org/10.1130/G37937.1
- Brand, U., Davis, A.M., Shaver, K.K., Blamey, N.J.F., Heizler, M., Lécuyer, C., 2021.
 Atmospheric oxygen of the Paleozoic. Earth-Sci. Rev. 216, 103560.
 https://doi.org/10.1016/j.earscirev.2021.103560

609

610

611

612

619

620

621

622

623

624

625

626

627

628

629

630

631

632

633

- Brimblecombe, P., 1996. Air Composition and Chemistry | Atmospheric science and meteorology, 2nd Ed. ed, Cambridge Environmental Chemistry Series. Cambridge University Press.
- Cerling, T.E., 1995. Stable Carbon Isotopes in Palaeosol Carbonates, in: Thiry, M., Simon-Coinçon, R. (Eds.), Palaeoweathering, Palaeosurfaces and Related Continental Deposits. Wiley, pp. 43–60. https://doi.org/10.1002/9781444304190.ch2
- Chayes, F., 1960. On correlation between variables of constant sum. J. Geophys. Res. 1896-1977 65, 4185–4193. https://doi.org/10.1029/JZ065i012p04185
- Chen, J., Zhang, X., Li, S., 2018. Heteroskedastic linear regression model with compositional response and covariates. J. Appl. Stat. 45, 2164–2181. https://doi.org/10.1080/02664763.2017.1413075
- Davis, A.M., 2018. Atmospheric and environmental interpretations of Early Paleozoic halite (Upper Ordovician, Hudson Bay Basin, & Upper Silurian, Michigan Basin).
- Deines, P., Langmuir, D., Harmon, R.S., 1974. Stable carbon isotope ratios and the existence of a gas phase in the evolution of carbonate ground waters. Geochim. Cosmochim. Acta 38, 1147–1164. https://doi.org/10.1016/0016-7037(74)90010-6
- Denk, T.R.A., Mohn, J., Decock, C., Lewicka-Szczebak, D., Harris, E., Butterbach-Bahl, K., Kiese, R., Wolf, B., 2017. The nitrogen cycle: A review of isotope effects and isotope modeling approaches. Soil Biol. Biochem. 105, 121–137. https://doi.org/10.1016/j.soilbio.2016.11.015
- Eggleston, S., Schmitt, J., Bereiter, B., Schneider, R., Fischer, H., 2016. Evolution of the
 stable carbon isotope composition of atmospheric CO2 over the last glacial cycle.
 Paleoceanography 31, 434–452. https://doi.org/10.1002/2015PA002874

- Farquhar, G.D., Ehleringer, J.R., Hubick, K.T., 1989. Carbon Isotope Discrimination and
 Photosynthesis. Annu. Rev. Plant Biol. 40, 503–537.
 https://doi.org/10.1146/annurev.pp.40.060189.002443
- Freyer, H.D., Wagener, K., 1975. Review on present results on fossil atmospheric gases trapped in evaporites. Pure Appl. Geophys. 113, 403–418. https://doi.org/10.1007/BF01592927
- Frezzotti, M.L., Tecce, F., Casagli, A., 2012. Raman spectroscopy for fluid inclusion
 analysis. J. Geochem. Explor. 112, 1–20.
 https://doi.org/10.1016/j.gexplo.2011.09.009

655 656

657

658

659

660

- Garcia, A.K., Cavanaugh, C.M., Kacar, B., 2021. The curious consistency of carbon
 biosignatures over billions of years of Earth-life coevolution. ISME J. 15, 2183–2194.
 https://doi.org/10.1038/s41396-021-00971-5
 - Golan, R., Lazar, B., Wurgaft, E., Lensky, N., Ganor, J., Gavrieli, I., 2017. Continuous CO2 escape from the hypersaline Dead Sea caused by aragonite precipitation. Geochim. Cosmochim. Acta 207, 43–56. https://doi.org/10.1016/j.gca.2017.02.031
 - Hudgins, M.N., Park, J.G., Ryan, A.M., Rogers, J.A., Schaller, M.F., In Review. Assessing the plausibility of direct constraints on ancient atmospheric pCO2 from fluid inclusions in halite: A theoretical and experimental approach.
 - Krissansen-Totton, J., Buick, R., Catling, D.C., 2015. A statistical analysis of the carbon isotope record from the Archean to Phanerozoic and implications for the rise of oxygen. Am. J. Sci. 315, 275–316. https://doi.org/10.2475/04.2015.01
- 663 Landis, G.P., Berner, R.A., 2018. Analysis of gases in fossil amber. Am. J. Sci. 318, 590–601. 664 https://doi.org/10.2475/05.2018.06
- LaRowe, D.E., Van Cappellen, P., 2011. Degradation of natural organic matter: A
 thermodynamic analysis. Geochim. Cosmochim. Acta 75, 2030–2042.
 https://doi.org/10.1016/j.gca.2011.01.020
- Lowenstein, T.K., Schubert, B.A., Timofeeff, M.N., 2011. Microbial communities in fluid inclusions and long-term survival in halite. GSA Today 21, 4–9. https://doi.org/10.1130/GSATG81A.1
- 671 Marty, B., Zimmermann, L., Pujol, M., Burgess, R., Philippot, P., 2013. Nitrogen Isotopic 672 Composition and Density of the Archean Atmosphere. Science 342, 101–104. 673 https://doi.org/10.1126/science.1240971
- Mills, B.J.W., Krause, A.J., Jarvis, I., Cramer, B.D., 2023. Evolution of Atmospheric O2
 Through the Phanerozoic, Revisited. Annu. Rev. Earth Planet. Sci. 51, 253–276.
 https://doi.org/10.1146/annurev-earth-032320-095425
- NOAA, 2024. Trends in Atmospheric Carbon Doxide (CO2) [WWW Document]. NOAA Glob.
 Monit. Lab. URL https://gml.noaa.gov/ccgg/trends/global.html (accessed 9.20.24).
- Osterrothová, K., Jehlička, J., 2011. Investigation of biomolecules trapped in fluid inclusions inside halite crystals by Raman spectroscopy. Spectrochim. Acta. A. Mol. Biomol. Spectrosc. 83, 288–296. https://doi.org/10.1016/j.saa.2011.08.032
- Park, J.G., Hudgins, M.N., Fralick, P.W., Shelley, J.T., Schaller, M.F., Accepted. Breathing Life into the Boring Billion: Direct Constraints From 1.4 Ga Fluid Inclusions Reveal a Fair Climate and Oxygenated Atmosphere. Proc. Natl. Acad. Sci.

- Park, J.G., Schaller, M.F., 2025. Constraints on Earth's atmospheric evolution from a gasaqueous partition of fluid inclusion volatiles. Gondwana Res. 139, 204–215. https://doi.org/10.1016/j.gr.2024.12.003
- Pettitt, E.A., Cherniak, D.J., Schaller, M.F., Watson, E.B., 2020. Diffusive retention of carbon and nitrogen in a microcrystalline quartz-dominated chert: Implications for reconstructing Earth's ancient atmosphere. Chem. Geol. 541, 119572. https://doi.org/10.1016/j.chemgeo.2020.119572
- 692 Pettitt, E.A., Schaller, M.F., 2020. A new calibration technique for quantitative gas analyses 693 of fluid inclusions using a quadrupole mass spectrometer. Rapid Commun. Mass 694 Spectrom. 34, e8855. https://doi.org/10.1002/rcm.8855
- Pingitore, N.E., Engle, M.A., 2022. Compositional Closure—Its Origin Lies Not in Mathematics but Rather in Nature Itself. Minerals 12, 74. https://doi.org/10.3390/min12010074
- 698 Rama, S.N.I., Hart, S.R., Roedder, E., 1965. Excess radiogenic argon in fluid inclusions. J. Geophys. Res. 1896-1977 70, 509–511. https://doi.org/10.1029/JZ070i002p00509
- Raynaud, D., Chowdhry Beeman, J., Chappellaz, J., Parrenin, F., Shin, J., 2020. Chapter 2 Antarctic air bubbles and the long-term ice core record of CO2 and other
 greenhouse gases, in: Oliva, M., Ruiz-Fernández, J. (Eds.), Past Antarctica.
 Academic Press, pp. 27–50. https://doi.org/10.1016/B978-0-12-817925-3.00002-1
- Roedder, E., 1984a. Fluid inclusions, Reviews in Mineralogy and Geochemistry.
 Mineralogical Association of America.
- 706 Roedder, E., 1984b. The fluids in salt. Am. Mineral. 69, 413–439.
- Rubino, M., Etheridge, D.M., Trudinger, C.M., Allison, C.E., Battle, M.O., Langenfelds, R.L.,
 Steele, L.P., Curran, M., Bender, M., White, J.W.C., Jenk, T.M., Blunier, T., Francey,
 R.J., 2013. A revised 1000 year atmospheric δ13C-CO2 record from Law Dome and
 South Pole, Antarctica. J. Geophys. Res. Atmospheres 118, 8482–8499.
 https://doi.org/10.1002/jgrd.50668
- Sander, R., 2023. Compilation of Henry's law constants (version 5.0.0) for water as solvent.

 Atmospheric Chem. Phys. 23, 10901–12440. https://doi.org/10.5194/acp-23-10901-
- Sano, Y., Pillinger, C.T., 1990. Nitrogen isotopes and N₂/Ar ratios in cherts: An attempt to
 measure time evolution of atmospheric δ¹⁵N value. Geochem. J. 24, 315–325.
 https://doi.org/10.2343/geochemj.24.315
- Schoenherr, J., Urai, J.L., Kukla, P.A., Littke, R., Schléder, Z., Larroque, J.-M., Newall, M.J.,
 Al-Abry, N., Al-Siyabi, H.A., Rawahi, Z., 2007. Limits to the sealing capacity of rock
 salt: A case study of the infra-Cambrian Ara Salt from the South Oman salt basin.
 AAPG Bull. 91, 1541–1557. https://doi.org/10.1306/06200706122
- Schreder-Gomes, S.I., Benison, K.C., Bernau, J.A., 2022. 830-million-year-old
 microorganisms in primary fluid inclusions in halite. Geology 50, 918–922.
 https://doi.org/10.1130/G49957.1
- Shatkay, M., Anati, D.A., Gat, J.R., 1993. Dissolved oxygen in the Dead Sea—seasonal
 changes during the holomictic stage. Int. J. Salt Lake Res. 2, 93–110.
 https://doi.org/10.1007/BF02905903

728 Shaver, K., 2018. Atmospheric conditions during the Visean (Carboniferous), and post-729 depositional hydrocarbon generation in the Shubenacadie Basin, Nova Scotia. Steinthorsdottir, M., Montañez, I.P., Royer, D.L., Mills, B.J.W., Hönisch, B., 2025. 730 731 Phanerozoic atmospheric CO2 reconstructed with proxies and models: Current 732 understanding and future directions. Treatise Geochem. 467–492. 733 The Cenozoic CO2 Proxy Integration Project (CENCO2PIP) Consortium, 2023. Toward a 734 Cenozoic history of atmospheric CO2. Science 382, eadi5177. 735 https://doi.org/10.1126/science.adi5177 736 Vreeland, R.H., Rosenzweig, W.D., Powers, D.W., 2000. Isolation of a 250 million-year-old 737 halotolerant bacterium from a primary salt crystal. Nature 407, 897–900. 738 https://doi.org/10.1038/35038060 Winters, Y. d., Lowenstein, T. k., Timofeeff, M. n., 2013. Identification of Carotenoids in 739 740 Ancient Salt from Death Valley, Saline Valley, and Searles Lake, California, Using 741 Laser Raman Spectroscopy. Astrobiology 13, 1065–1080. 742 https://doi.org/10.1089/ast.2012.0952 743 Yeung, L.Y., 2017. Low oxygen and argon in the Neoproterozoic atmosphere at 815 Ma. 744 Earth Planet. Sci. Lett. 480, 66-74. https://doi.org/10.1016/j.epsl.2017.09.044 745 Zhang, J., Quay, P.D., Wilbur, D.O., 1995. Carbon isotope fractionation during gas-water exchange and dissolution of CO2. Geochim. Cosmochim. Acta 59, 107–114. 746 747 https://doi.org/10.1016/0016-7037(95)91550-D

Supporting Information for "A First Principles Critique of the Back Calculation Method: Understanding and Assessing the Alteration of Atmospheric Gases Trapped in Ancient Fluid Inclusions"

Authors: Justin G. Park^{1,2}, Morgan F. Schaller^{1,2}

Affiliations:

- 1. Department of Earth and Environmental Sciences, Rensselaer Polytechnic Institute, Troy, New York. 12180
- 2. Center for Environmental and Stable Isotope Analysis, Rensselaer Polytechnic Institute, Troy, New York. 12180

S1.0 Deriving Relationships between Partitioned Gases

The relationship between partitioned O_2 and CO_2 mole fractions ($X_{O_2}^p$ and $X_{CO_2}^p$) is derived very similarly to the relationship between raw mole fractions. We begin with equation 18 as presented in the main text:

$$X_{i}^{p} = \frac{\frac{n_{i}^{t} + \Delta n_{i}}{Y_{i}\left(\varphi_{g}, T, S\right)}}{\sum_{j \in J} \frac{n_{j}^{t} + \Delta n_{j}}{Y_{j}\left(\varphi_{g}, T, S\right)}}$$
Eq. 18

Where n_i^t and Δn_i are the trapped and altered moles of a gas, and Y_i is the abbreviated term describing gas-aqueous equilibria, as defined in equation 2 in the main text. Rearranging equation 1 we obtain:

$$P_i V = \frac{n_i^t}{Y_i \left(\varphi_g, T, S\right)}$$
 Eq. S1

Where P_i is the atmospheric partial pressure of a gas and V is the volume of the inclusions. We present two identities:

$$P_{atm} = \sum_{j \in J} P_j$$
 Eq. S2

And:

$$X_i^{atm} = \frac{P_i}{P_{atm}}$$
 Eq. S3

Where J is the set of atmospheric gases. Partitioning attempts to determine P_iV for each gas, but alteration skews the apparent values:

$$P_i^p V = \frac{n_i^t + \Delta n_i}{Y_i(\varphi_g, T, S)}$$
 Eq. S4

If alteration is confined to only O_2 and CO_2 and the two are related through Q_a , their partitioned mole fractions can be obtained by substituting the relevant forms of equation S1 into equation 18:

$$X_{O_{2}}^{p} = \frac{P_{O_{2}}V + \frac{\Delta n_{CO_{2}}Q_{a}}{Y_{O_{2}}\left(\varphi_{g}, T, S\right)}}{P_{atm}V + \frac{\Delta n_{CO_{2}}Q_{a}}{Y_{O_{2}}\left(\varphi_{g}, T, S\right) + \frac{\Delta n_{CO_{2}}}{Y_{CO_{2}}\left(\varphi_{g}, T, S\right)}}$$
Eq. S5

And:

$$X_{CO_{2}}^{p} = \frac{P_{CO_{2}}V + \frac{\Delta n_{CO_{2}}}{Y_{CO_{2}}(\varphi_{g}, T, S)}}{P_{atm}V + \frac{\Delta n_{CO_{2}}Q_{a}}{Y_{O_{2}}(\varphi_{g}, T, S)} + \frac{\Delta n_{CO_{2}}}{Y_{CO_{2}}(\varphi_{g}, T, S)}}$$
 Eq. S6

These equations can be solved independently for the term $\Delta n_{CO2}/P_{atm}V$. After substituting in the appropriate form of equation S3, we obtain the forms:

$$\frac{\Delta n_{CO_2}}{P_{atm}V} = \frac{X_{O_2}^p - X_{O_2}^{atm}}{\frac{\left(1 - X_{O_2}^p\right)Q_a}{Y_{O_2}\left(\varphi_q, T, S\right)} - \frac{X_{O_2}^p}{Y_{CO_2}\left(\varphi_q, T, S\right)}} \tag{Eq. S7}$$

And:

$$\frac{\Delta n_{CO_2}}{P_{atm}V} = \frac{X_{CO_2}^p - X_{CO_2}^{atm}}{\frac{\left(1 - X_{CO_2}^p\right)}{Y_{CO_2}\left(\varphi_a, T, S\right)} - \frac{X_{CO_2}^pQ_a}{Y_{O_2}\left(\varphi_a, T, S\right)}}$$
Eq. S8

After dividing both equations by Y_{CO2} and substituting in the appropriate partition coefficient (β_{CO2-O2} , equation 17), we obtain the relationship:

$$\frac{X_{O_2}^p - X_{O_2}^{atm}}{\left(1 - X_{O_2}^p\right)\beta_{CO_2 - O_2}Q_a - X_{O_2}^p} = \frac{X_{CO_2}^p - X_{CO_2}^{atm}}{\left(1 - X_{CO_2}^p\right) - \beta_{CO_2 - O_2}X_{CO_2}^pQ_a}$$
Eq. S9

Setting $k = \beta_{CO2-O2}Qa$ and solving for $X_{O_2}^p$, we obtain equation 19:

$$X_{O_2}^p = \frac{X_{CO_2}^p \left[X_{O_2}^{atm}(k+1) - k \right] + \left[X_{CO_2}^{atm}k - X_{O_2}^{atm} \right]}{X_{CO_2}^{atm}(k+1) - 1}$$
 Eq. 19

This relationship is linear if k is constant.

S2.0 Isotopic Constraints on Inclusion CO₂

Stable carbon isotope analyses were performed on CO₂ released from several inclusion bearing halite samples. Three modern samples were analyzed, including halite collected in 2012 from Conti Vecchi (Italy), in 1994 from Death Valley, California (USA), and in 1980 from Baja California (Mexico). Additionally, two ancient samples were analyzed, including 69 ka. halite from the Atacama Desert (Chile) and 1.44 Ga. halite from the Sibley Group, Ontario (Canada). Samples selected for analyses demonstrated clear evidence of primary growth structures (see Blamey and Brand, 2019), and the inclusions contained variable volumes of trapped air bubbles. The Sibley halite, including this sample, are described in detail in Park et al., (Accepted).

For each sample, approximately 100 mg of primary halite was loaded into a stainless steel crusher (Pettitt and Schaller, 2020) attached to an Elementar Isoprime 100 Dual Inlet Isotope Ratio Mass Spectrometer (DI-IRMS; Elementar Americas Inc., Ronkonkoma, NY, USA). Samples were pumped to high vacuum ($\sim 10^{-7}$ to 10^{-8} mbar) and crushed to release the trapped gases. Cryogenic separation was used to collect the released CO₂ and separate it from the remainder of the inclusion gases. The released inclusion water was initially trapped in a -80 °C water trap, with subsequent CO₂ trapping in a -180 °C cold finger. At this stage the noncondensable gases were evacuated. The CO₂ was then released by warming the cold finger to -80 °C and recollected in a second cold finger closer to the analyzer. Approximately 10 minutes was spent at each stage. CO₂ entering the analyzer was ionized by electron ionization and accelerated toward high sensitivity faraday cups to measure m/z 44, 45, and 46. During analysis the instrument alternated between measuring the sample CO₂ and a reference CO₂ (δ^{13} C = 5.018 ± 0.005% and $\delta^{18}O = -5.80 \pm 0.01\%$, VPDB) that is regularly checked against NIST NBS19 (12 comparisons of 10 seconds each). Craig corrections were used to track the relative influence of isobaric interferences (Craig, 1957). Sample ion beams ranged in size from 5 to 50 pA, with the smaller beams yielding increased uncertainty. All results can be found in Table S1.

Atmospheric δ^{13} C values were obtained from well document modern and ancient sources. Values for the Baja California, Death Valley, and Conti Vecchi Halite were obtained from modern measurements through the Isotopic Data Gallery from the the Scripps CO₂ Program

(https://scrippsco2.ucsd.edu/). The 69 ka value for the Atacama halite was obtained from $\delta^{13}C$ measurements of CO_2 in glacial ice, largely from the Talos Dome region of Antarctica (Eggleston et al., 2016). The $\delta^{13}C_{atm}$ of 1.44 Ga was estimated from marine carbonate records formed 1.35 to 1.55 billion years ago. The binned $\delta^{13}C_{carb}$ values vary between -3‰ and 0.809‰, and modeled estimates from Kernal and Lowess smoothing yield $\delta^{13}C_{carb}$ between -1.25‰ and 0.3‰ (Krissansen-Totton et al., 2015). From these numbers, standard isotopic fractions (i.e. approximately 8‰ between atmospheric CO_2 and carbonate minerals; Deines et al., 1974; Zhang et al., 1995) predict the $\delta^{13}C_{atm}$ was in the range of -7.7‰ to -9.25‰. This range overlaps with the measured $\delta^{13}C$ recorded by the Sibley halite CO_2 (Park et al., Accepted). Accordingly, a value of -8‰ was used for calculations.

Table S1: Stable isotope ratios are compared for CO₂ released from halite fluid inclusions.

Halite Source	Age	Mass (mg)	m/z 44 Beam (pA)	δ^{13} C (‰, VPDB)
Conti Vecchi (Italy)	2012	57.045	4.95*	-15.560±1.609
Death Valley (USA)	1994	132.312	34.7	-25.601±0.336
Baja California (Mexico)	1980	127.134	40.4	-23.384 ± 0.272
Atacama Desert (Chile)	69 ka.	101.376	39.1	-20.087±0.153
Sibley Group (Canada)	1.44 Ga.	114.890	53.3	-8.377 ± 0.196

^{*}Craig correction not applied due to size limitations

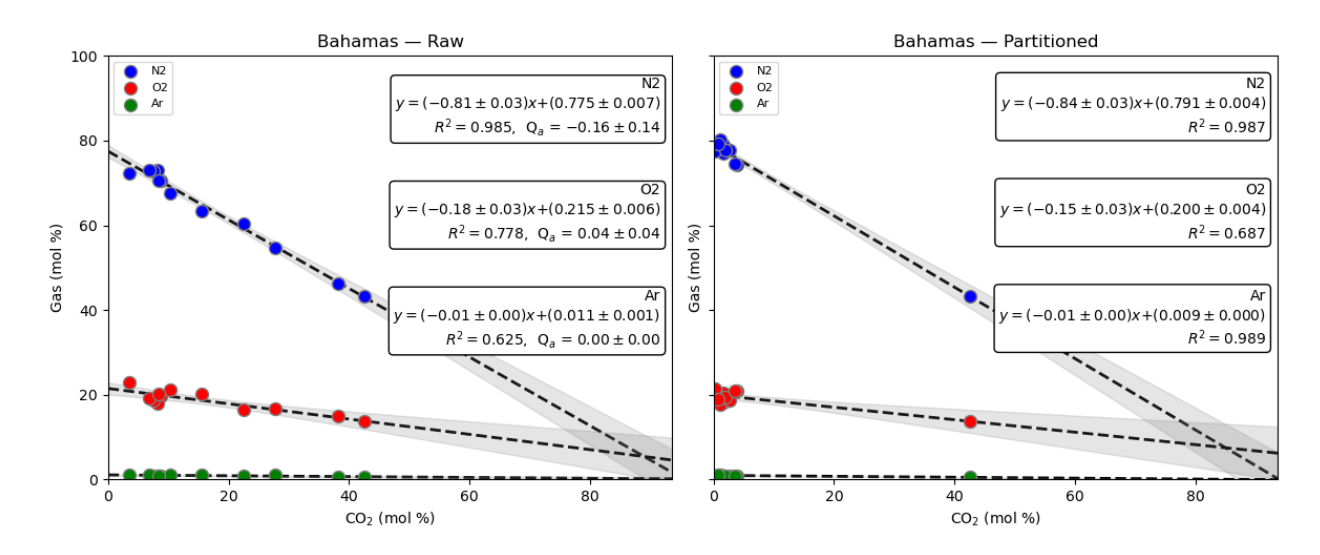


Figure S1: Gas data from modern halite inclusion from the Bahamas are evaluated through the back calculation method. Regressions are fit to paired mole fractions of N₂ vs. CO₂ (blue), O₂ vs. CO₂ (red), and Ar Vs. CO₂, for both raw (Left) and partitioned (Right) mole fractions. Data is retrieved from (Blamey and Brand, 2019; Brand et al., 2021).

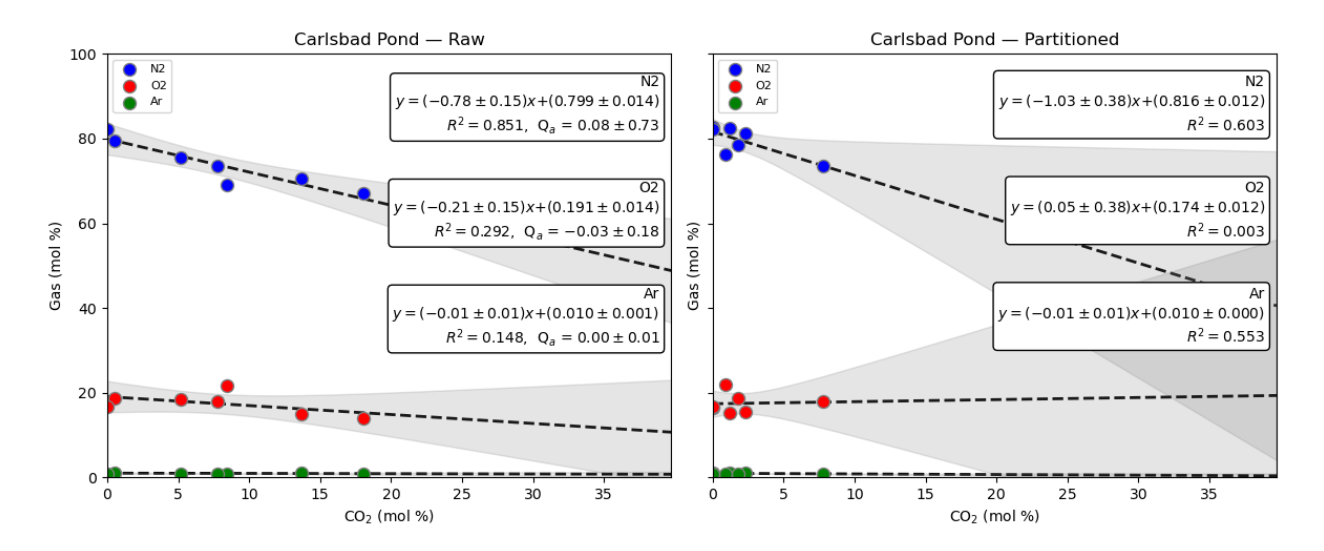


Figure S2: Gas data from modern halite inclusion from Carlsbad Pond (USA) are evaluated through the back calculation method. Regressions are fit to paired mole fractions of N₂ vs. CO₂ (blue), O₂ vs. CO₂ (red), and Ar Vs. CO₂, for both raw (Left) and partitioned (Right) mole fractions. Data is retrieved from (Blamey and Brand, 2019; Brand et al., 2021).

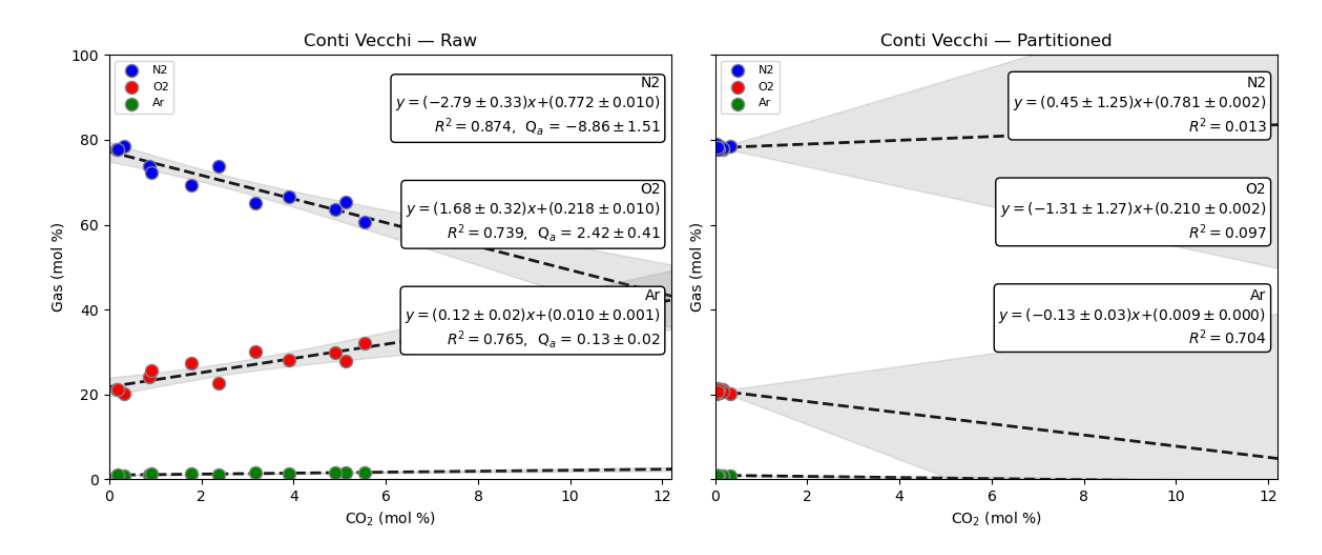


Figure S3: Gas data from modern halite inclusion from Conti Vecchi (Italy) are evaluated through the back calculation method. Regressions are fit to paired mole fractions of N₂ vs. CO₂ (blue), O₂ vs. CO₂ (red), and Ar Vs. CO₂, for both raw (Left) and partitioned (Right) mole fractions. Data is retrieved from (Park and Schaller, 2025).

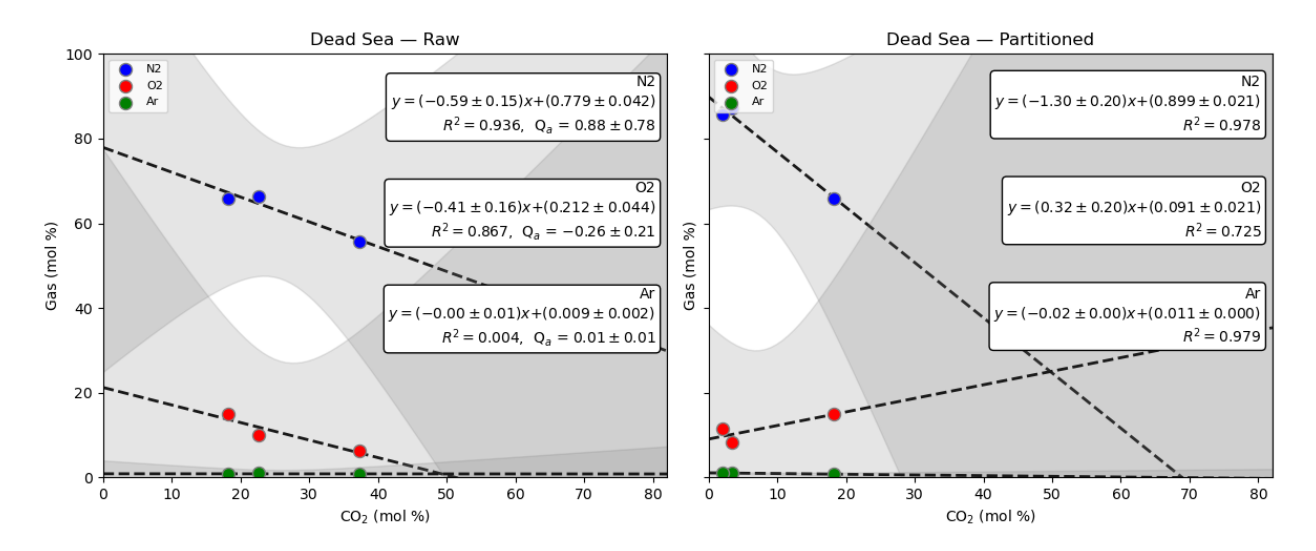


Figure S4: Gas data from modern halite inclusion from the Dead Sea (Israel) are evaluated through the back calculation method. Regressions are fit to paired mole fractions of N₂ vs. CO₂ (blue), O₂ vs. CO₂ (red), and Ar Vs. CO₂, for both raw (Left) and partitioned (Right) mole fractions. Data is retrieved from (Blamey and Brand, 2019; Brand et al., 2021).

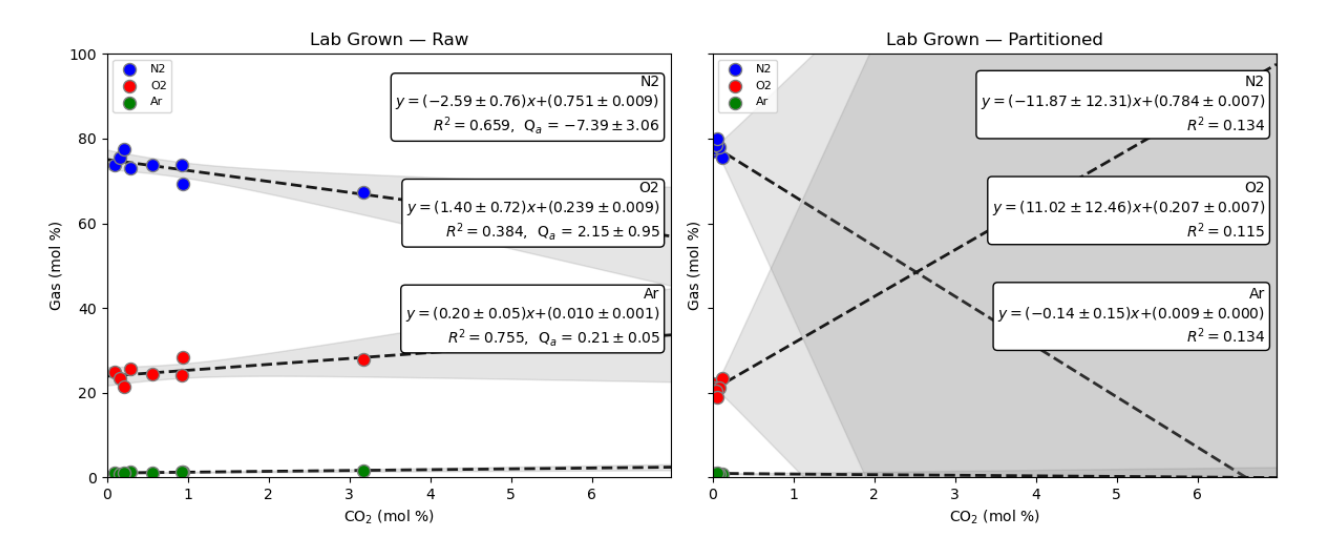


Figure S5: Gas data from lab grown halite inclusion are evaluated through the back calculation method. Regressions are fit to paired mole fractions of N₂ vs. CO₂ (blue), O₂ vs. CO₂ (red), and Ar Vs. CO₂, for both raw (Left) and partitioned (Right) mole fractions. Data is retrieved from(Park and Schaller, 2025).

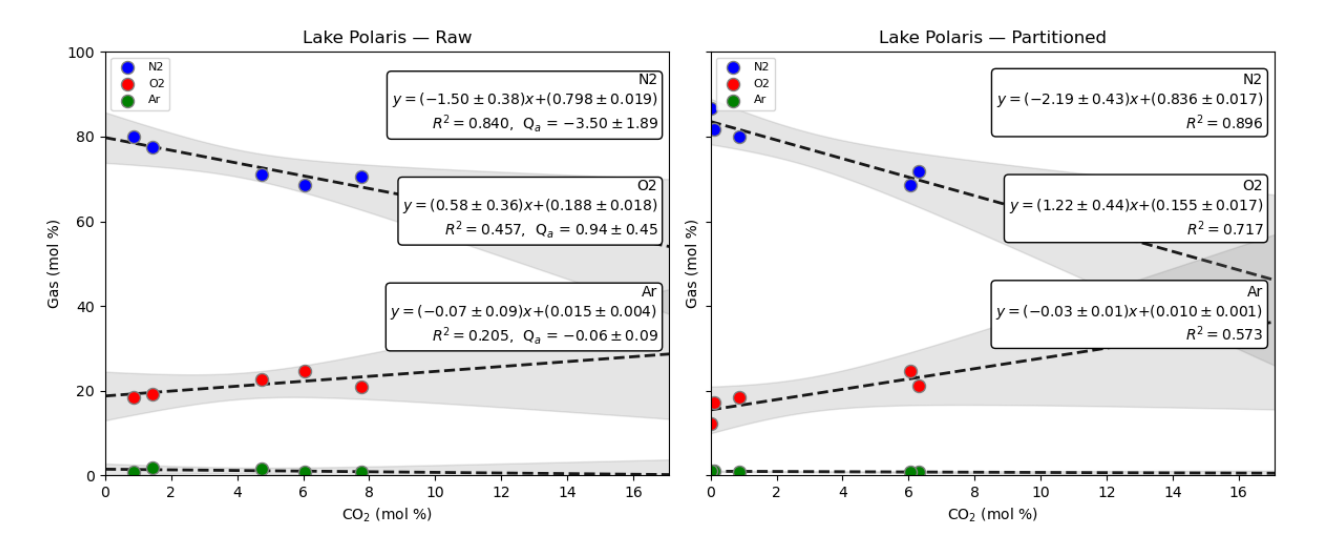


Figure S6: Gas data from modern halite inclusion from Lake Polaris (Australia) are evaluated through the back calculation method. Regressions are fit to paired mole fractions of N₂ vs. CO₂ (blue), O₂ vs. CO₂ (red), and Ar Vs. CO₂, for both raw (Left) and partitioned (Right) mole fractions. Data is retrieved from (Blamey and Brand, 2019; Brand et al., 2021).

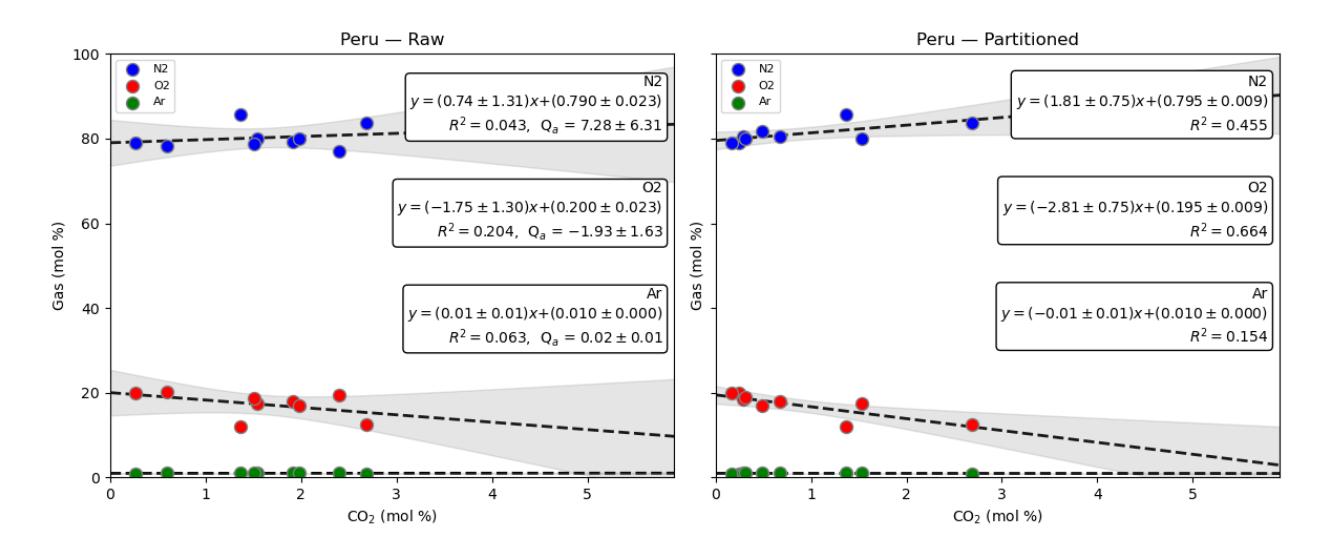


Figure S7: Gas data from modern halite inclusion from Peru are evaluated through the back calculation method. Regressions are fit to paired mole fractions of N₂ vs. CO₂ (blue), O₂ vs. CO₂ (red), and Ar Vs. CO₂, for both raw (Left) and partitioned (Right) mole fractions. Data is retrieved from (Blamey and Brand, 2019; Brand et al., 2021).

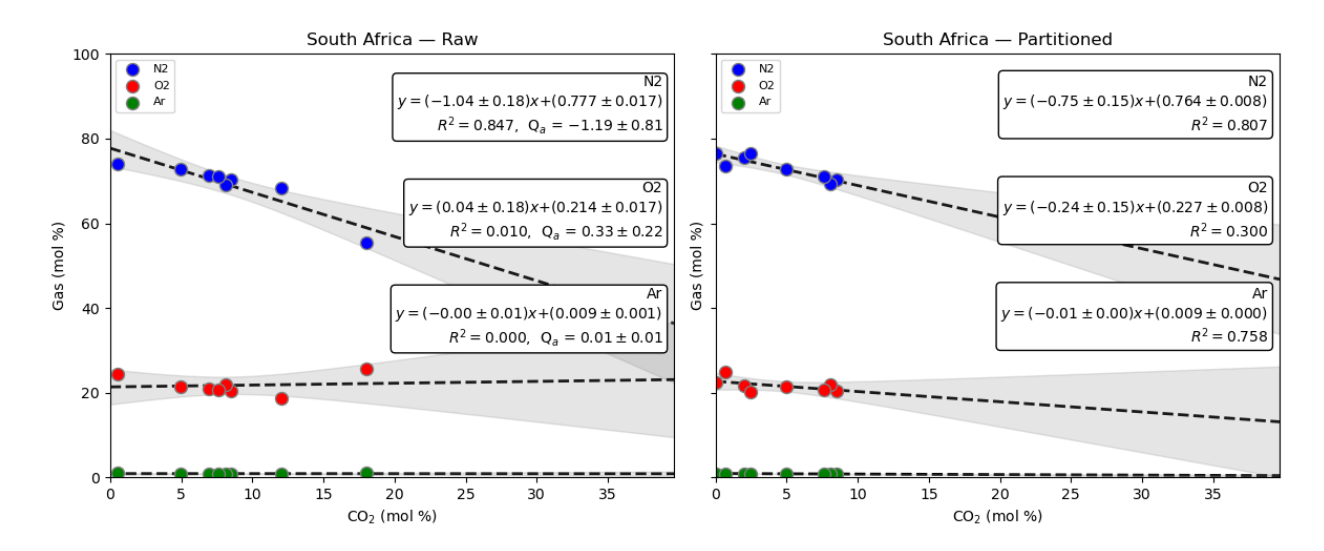


Figure S8: Gas data from modern halite inclusion from South Africa are evaluated through the back calculation method. Regressions are fit to paired mole fractions of N₂ vs. CO₂ (blue), O₂ vs. CO₂ (red), and Ar Vs. CO₂, for both raw (Left) and partitioned (Right) mole fractions. Data is retrieved from (Blamey and Brand, 2019; Brand et al., 2021).

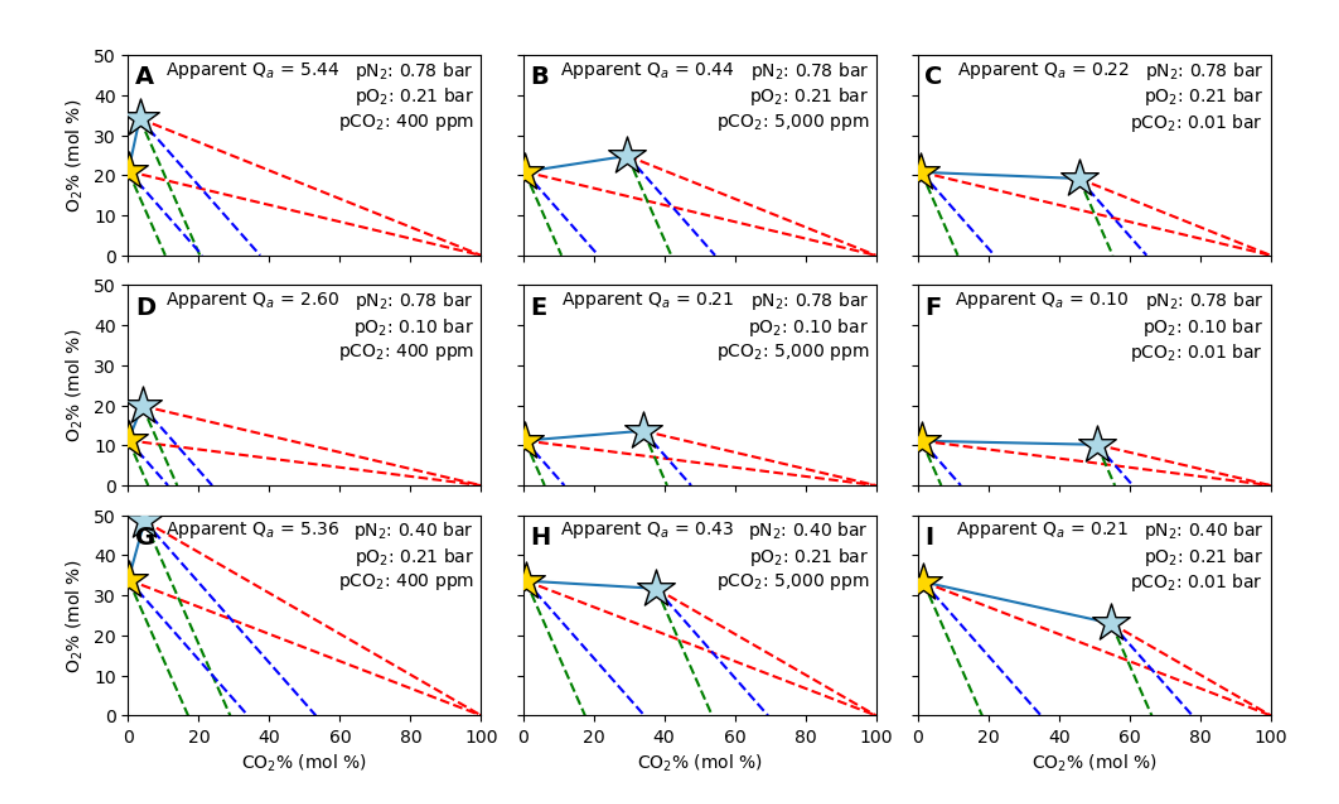


Figure S9: Fluid inclusion gas compositions are modeled for mixtures of a variety of atmospheric compositions (gold stars) and air saturated brines (blue stars). For each row the partial pressure of N_2 or O_2 changes relative to modern atmosphere levels: (A-C) modern atmosphere levels, (D-F) ~ 0.5 times modern O_2 levels, (G-I) ~ 0.5 times modern O_2 levels. The partial pressure of O_2 increases across columns. Modeled mixing lines yield positive and negative slopes, yet the apparent alteration quotient (O_2) is always positive.

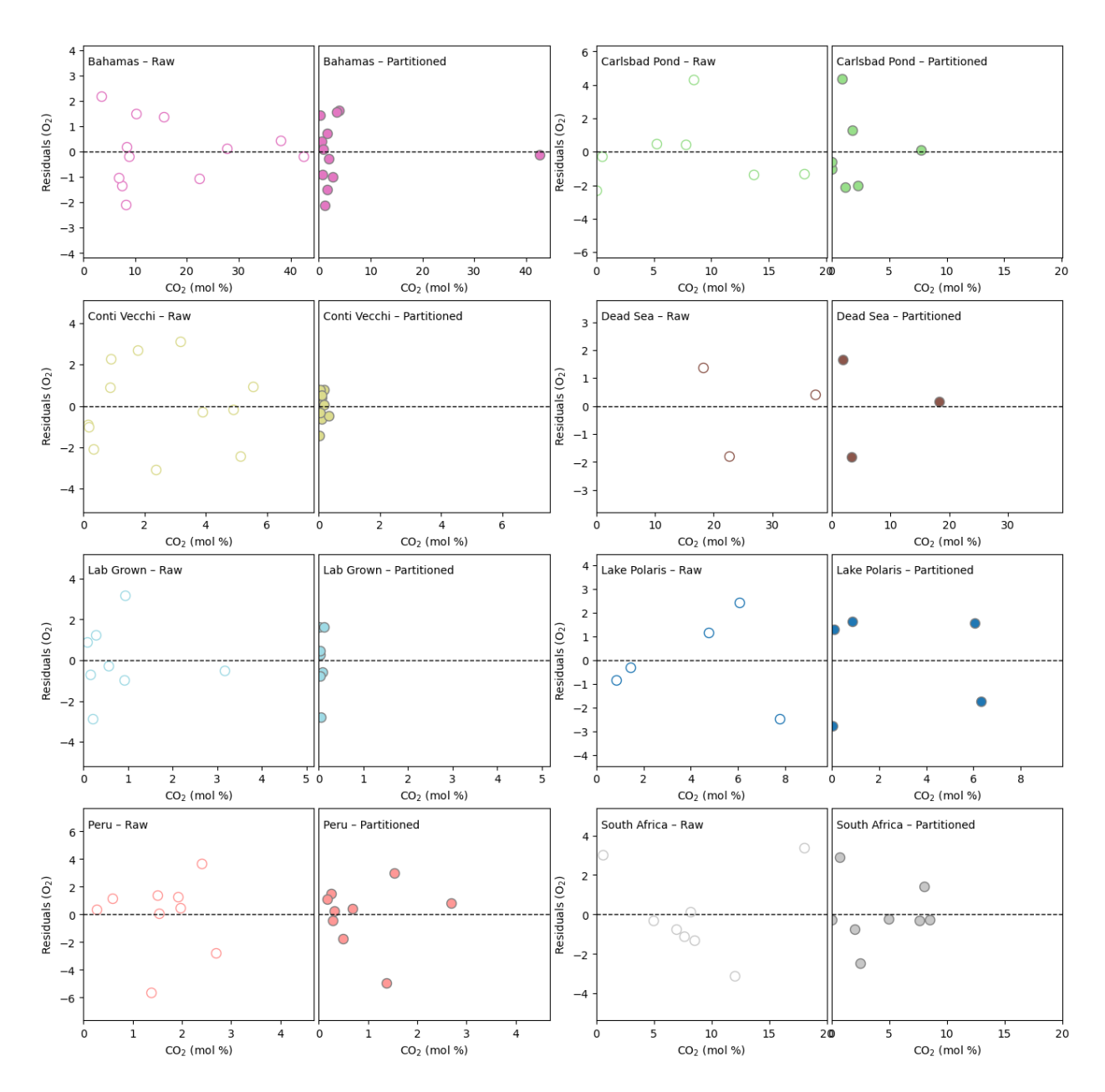


Figure S10: The residuals of BCM regressions through modern halite gases are compared. For each locality, the left plot shows residuals for the raw gases and the right for partitioned gases. Some residuals through the raw data display evidence of heteroskedasticity (e.g., Bahamas-Raw) or larger unaccounted for trends (e.g., Lake Polaris and South Africa). Data is sourced from (Blamey and Brand, 2019; Brand et al., 2021; Park and Schaller, 2025)

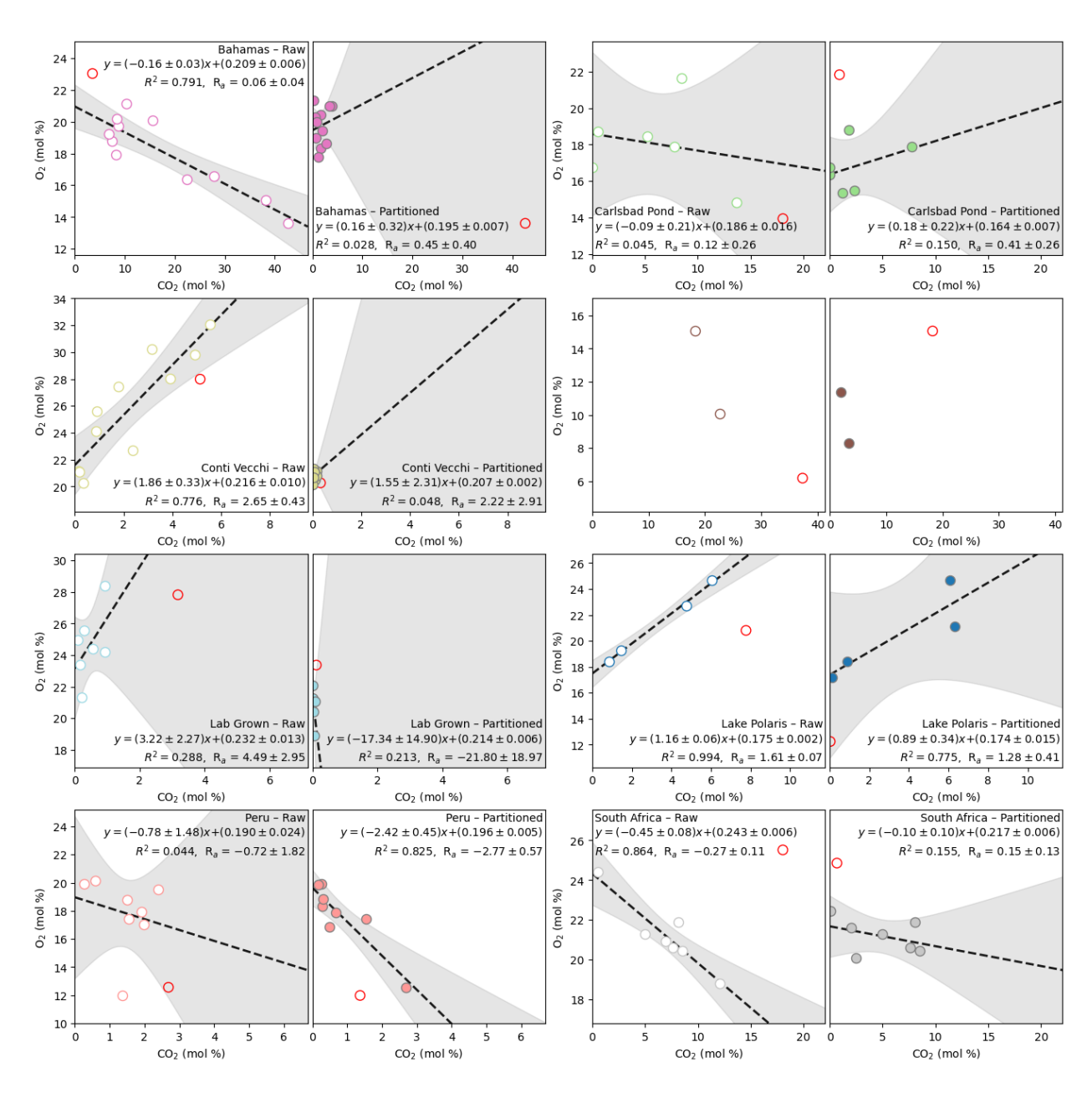


Figure S11: The BCM is reapplied to gas compositions from modern halite inclusions after removing the points with the highest Cook's distance from each locality (red circles). Each pair of plots represents the raw (left) and partitioned (right) data from the locality. Removal of these points has changed some regressions substantially (See Fig. 3). All data is sourced from (Blamey and Brand, 2019; Brand et al., 2021; Park and Schaller, 2025)

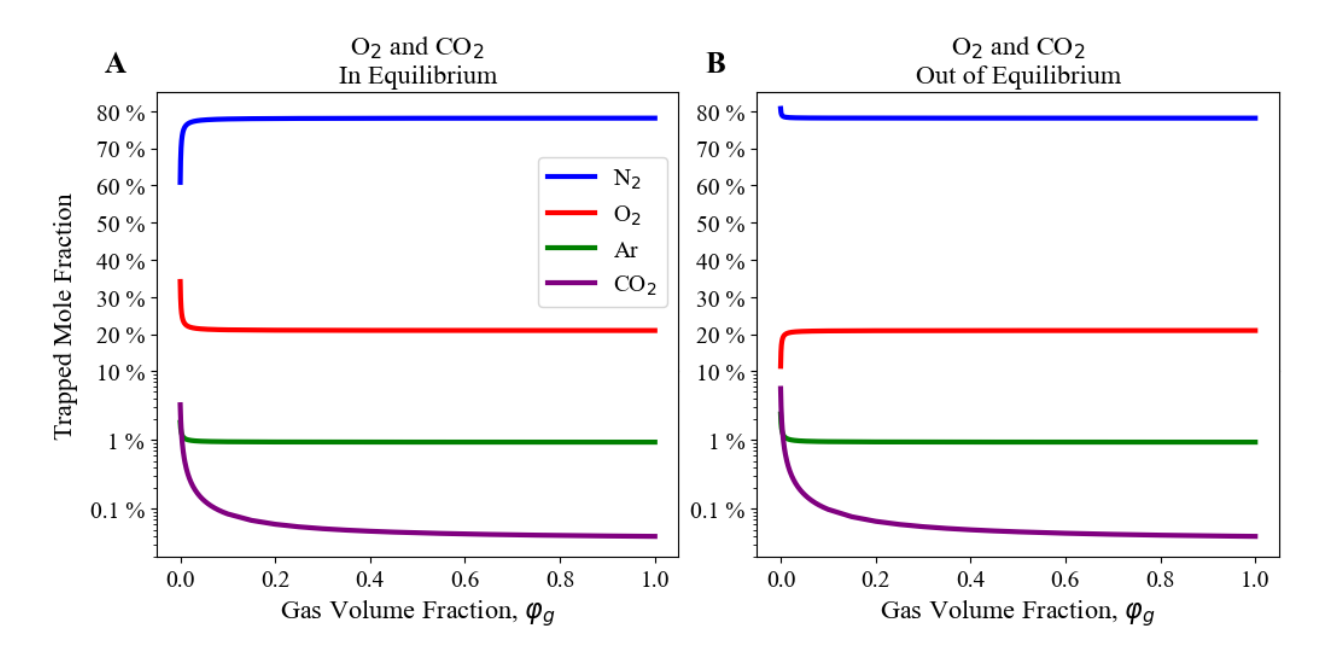


Figure S12: Inclusion gas compositions are modeled as a function of the gas volume fraction, ϕ_g , for two cases: A) a modern atmosphere in equilibrium with air saturated brines, and B) the same system, but O_2 and CO_2 are not in equilibrium. Both plots are computed using equation 2. The out of equilibrium model assumes dissolved O_2 concentrations are only a quarter of the expected values from O_2 's henry's solubility, whereas CO_2 is assumed to be 30% more concentrated than expected. The result skews the relative abundance of all gases at lower ϕ_g values, which will not produce true atmospheric composition when partitioned assuming expected solubilities. All calculations assume entrapment at 25 °C with a 7.5 M NaCl equivalent brine.

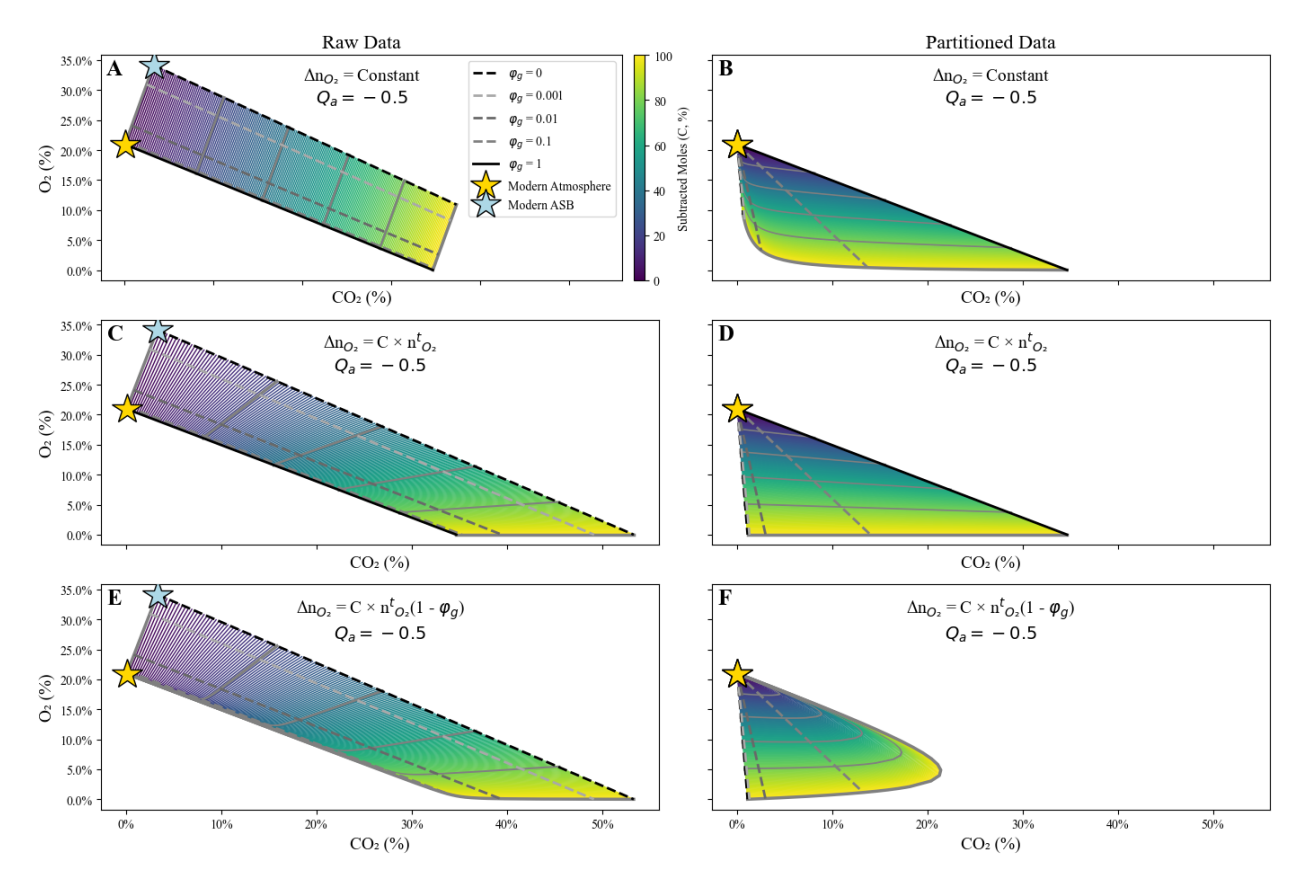


Figure S13: Possible fluid inclusion gas compositions are modeled for modern atmosphere (gold stars) mixing with air saturated brine (blue stars) with alteration acting upon the trapped gases with Q_a = -0.5. Alteration is modeled as (A & B) constant for all ϕ_g , (C & D) proportional to the trapped O_2 , and (E &F) proportional to the trapped O_2 multiplied by the brine volume fraction (i.e., 1- ϕ_g). The extent of the alteration is shown in a color scale. Solid grey lines reflect equal alteration extents. The dashed grey lines and the solid black lines are lines of equal ϕ_g . In raw data, only data with ϕ_g close to 1 are viable for the BCM. When partitioned, any set of data with consistent ϕ_g is viable.

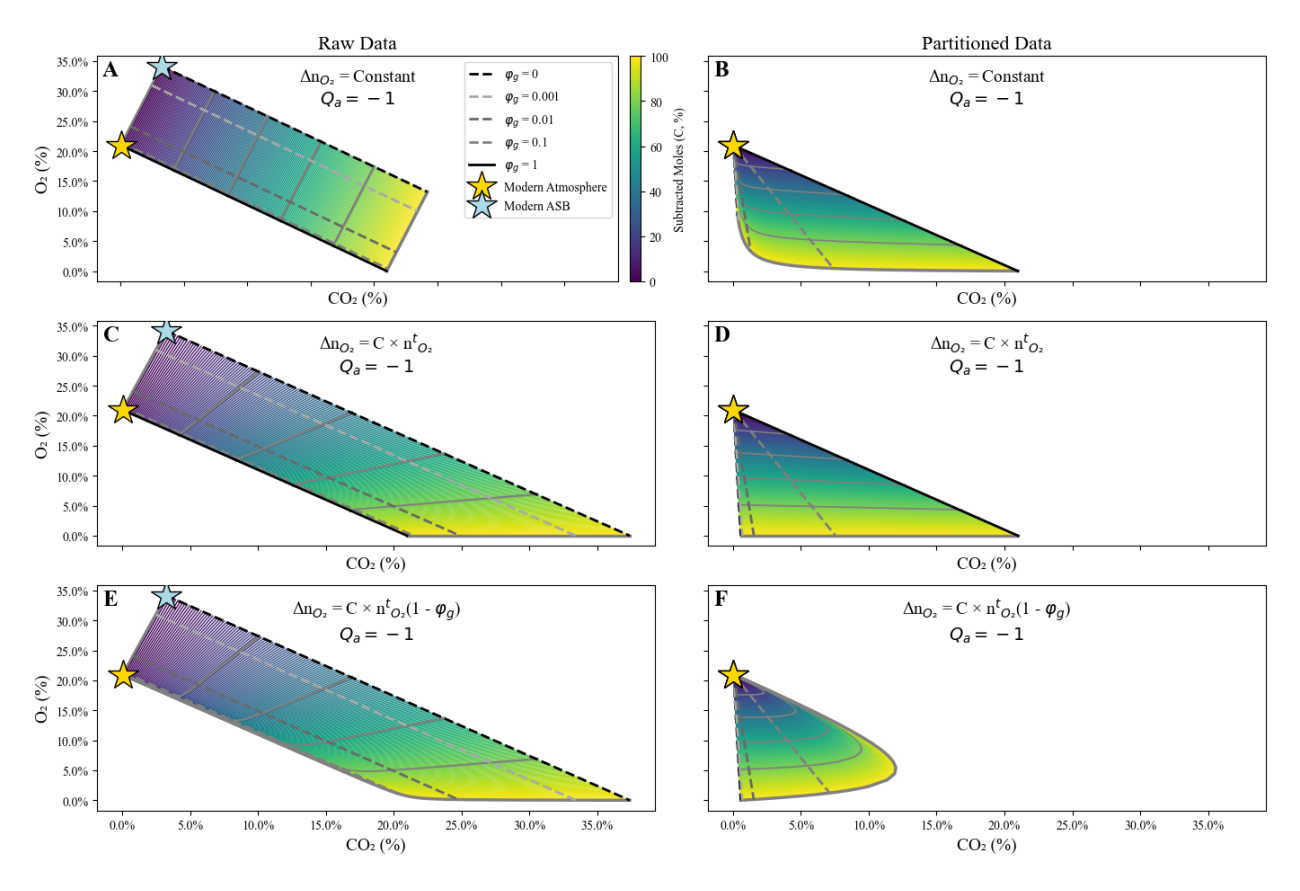


Figure S14: Possible gas compositions are modeled for fluid inclusions trapping variable volumes of air and brine, with alteration of $Q_a = -1$. Subplots are displayed similarly to Fig. S13, including lettering, color schemes, and alteration extents.

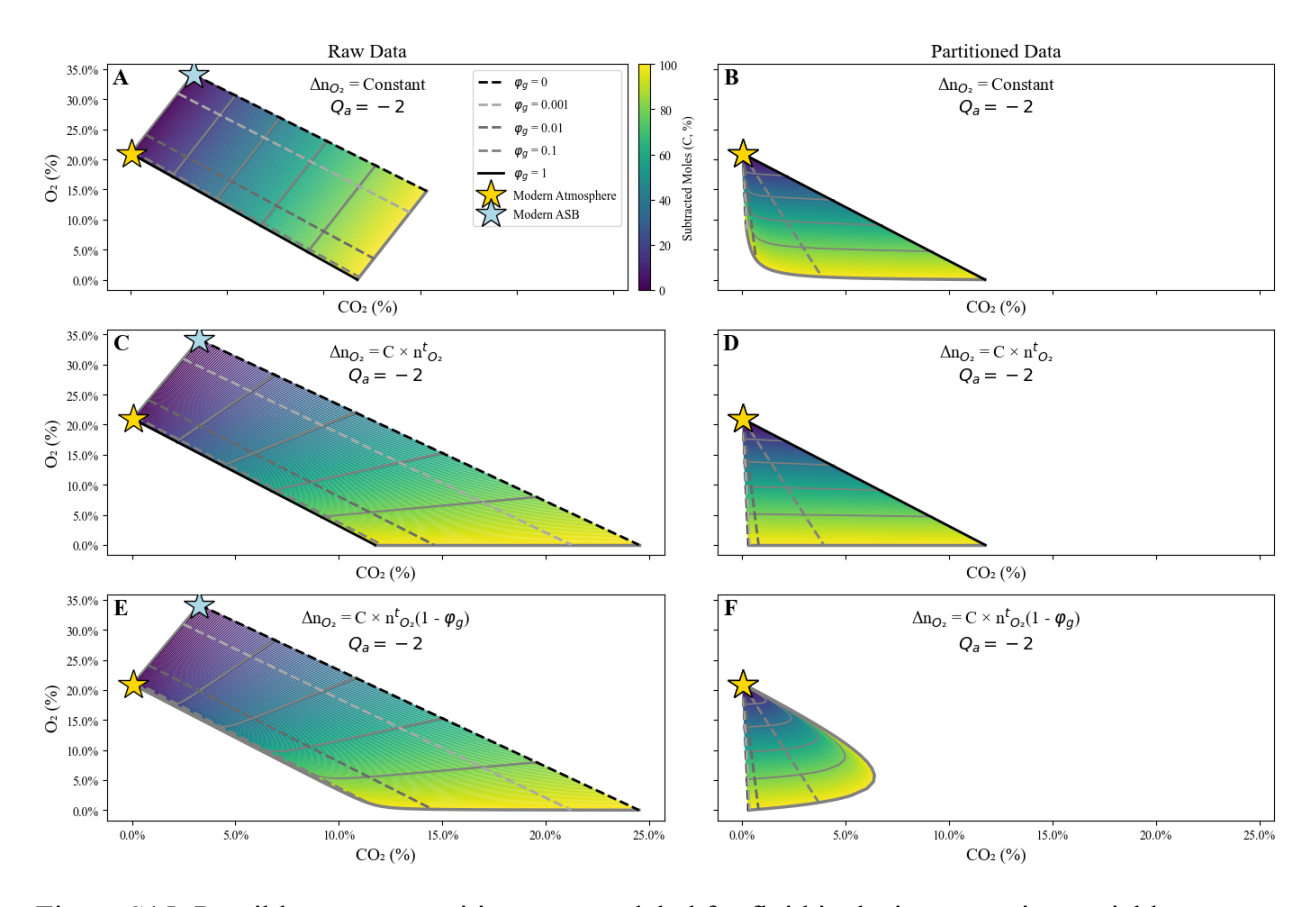


Figure S15: Possible gas compositions are modeled for fluid inclusions trapping variable volumes of air and brine, with alteration of $Q_a = -2$. Subplots are displayed similarly to Fig. S13, including lettering, color schemes, and alteration extents.

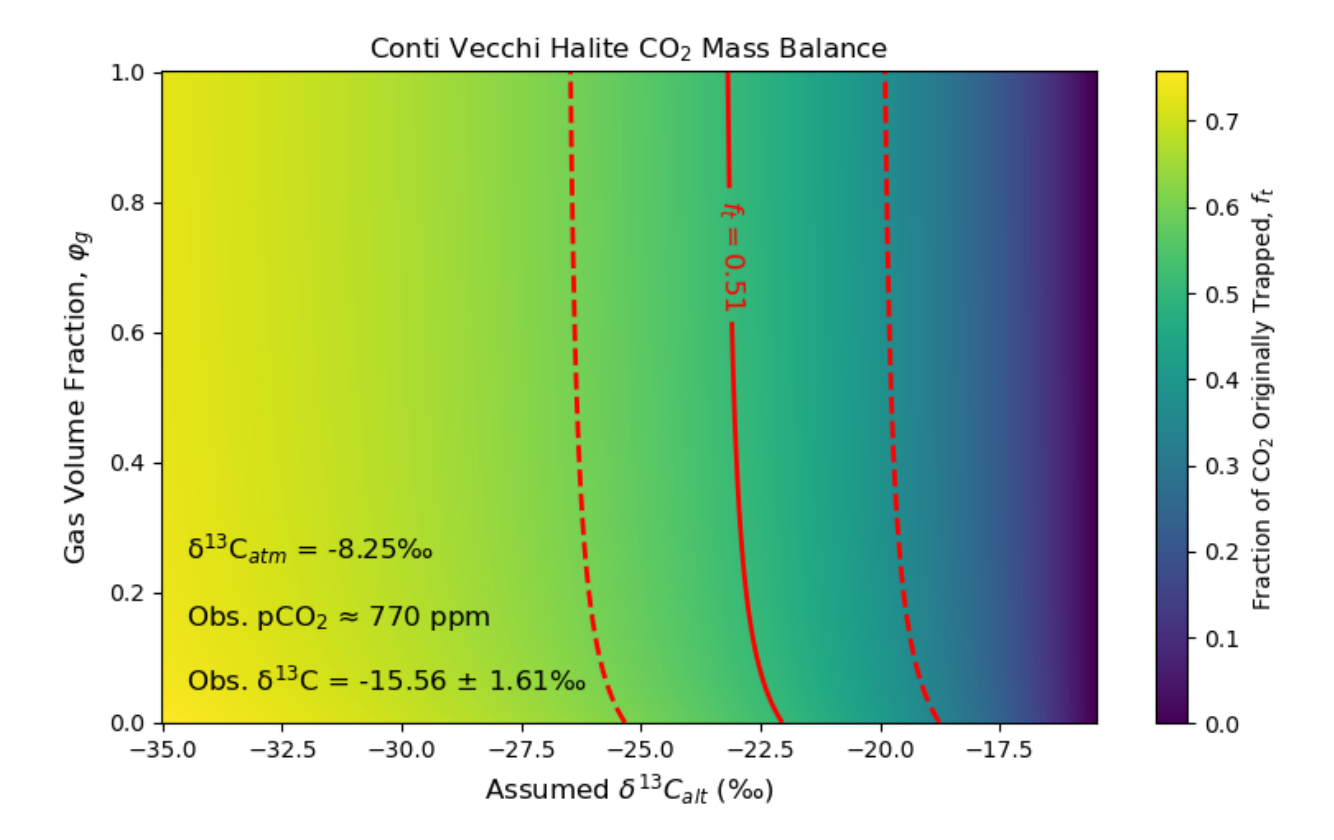


Figure S16: The fraction of CO₂ that was originally trapped (f_t) in the Conti Vecchi halite is calculated for various combinations of φ_g and $\delta^{13}C_{alt}$. A heat map shows f_t for each combination. The sold red line shows the combinations that yield $f_t = 0.51$, the necessary value to yield the recorded atmospheric pCO₂ in 2012 (0.51 = 393 ppm / 770 ppm). Dashed red lines reflect upper and lower bounds based on the uncertainty in the measured $\delta^{13}C$ of the inclusion CO₂ (this does not include the uncertainty of the pCO₂ measurements).

References:

- Blamey, N.J.F., Brand, U., 2019. Atmospheric gas in modern and ancient halite fluid inclusions: A screening protocol. Gondwana Res. 69, 163–176. https://doi.org/10.1016/j.gr.2018.12.004
- Brand, U., Davis, A.M., Shaver, K.K., Blamey, N.J.F., Heizler, M., Lécuyer, C., 2021. Atmospheric oxygen of the Paleozoic. Earth-Sci. Rev. 216, 103560. https://doi.org/10.1016/j.earscirev.2021.103560
- Craig, H., 1957. Isotopic standards for carbon and oxygen and correction factors for mass-spectrometric analysis of carbon dioxide. Geochim. Cosmochim. Acta 12, 133–149. https://doi.org/10.1016/0016-7037(57)90024-8
- Deines, P., Langmuir, D., Harmon, R.S., 1974. Stable carbon isotope ratios and the existence of a gas phase in the evolution of carbonate ground waters. Geochim. Cosmochim. Acta 38, 1147–1164. https://doi.org/10.1016/0016-7037(74)90010-6
- Eggleston, S., Schmitt, J., Bereiter, B., Schneider, R., Fischer, H., 2016. Evolution of the stable carbon isotope composition of atmospheric CO2 over the last glacial cycle. Paleoceanography 31, 434–452. https://doi.org/10.1002/2015PA002874
- Krissansen-Totton, J., Buick, R., Catling, D.C., 2015. A statistical analysis of the carbon isotope record from the Archean to Phanerozoic and implications for the rise of oxygen. Am. J. Sci. 315, 275–316. https://doi.org/10.2475/04.2015.01
- Park, J.G., Hudgins, M.N., Fralick, P.W., Shelley, J.T., Schaller, M.F., Accepted. Breathing Life into the Boring Billion: Direct Constraints From 1.4 Ga Fluid Inclusions Reveal a Fair Climate and Oxygenated Atmosphere. Proc. Natl. Acad. Sci.
- Park, J.G., Schaller, M.F., 2025. Constraints on Earth's atmospheric evolution from a gasaqueous partition of fluid inclusion volatiles. Gondwana Res. 139, 204–215. https://doi.org/10.1016/j.gr.2024.12.003
- Pettitt, E.A., Schaller, M.F., 2020. A new calibration technique for quantitative gas analyses of fluid inclusions using a quadrupole mass spectrometer. Rapid Commun. Mass Spectrom. 34, e8855. https://doi.org/10.1002/rcm.8855
- Zhang, J., Quay, P.D., Wilbur, D.O., 1995. Carbon isotope fractionation during gas-water exchange and dissolution of CO2. Geochim. Cosmochim. Acta 59, 107–114. https://doi.org/10.1016/0016-7037(95)91550-D